Ocean Engineering 257 (2022) 111618

Contents lists available at ScienceDirect

Ocean Engineering

journal homepage: www.elsevier.com/locate/oceaneng

Gain-scheduled steering control for a wave-propelled unmanned surface vehicle

Alberto Dallolio *, Henning Øveraas, Tor Arne Johansen

Centre for Autonomous Marine Operations and Systems, Department of Engineering Cybernetics, Norwegian University of Science and Technology (NTNU), O. S. Bragstads Plass 2D, Trondheim, 7034, Norway

ARTICLE INFO

Keywords:
Autonomous surface vehicles
Robotics
Control application
Experimental results

ABSTRACT

The persistent observation of oceanographic phenomena is nowadays hampered by technological limitations, that prevent marine robotic platforms to autonomously execute scientific surveys for extended periods of time. The propulsion and course-over-ground (COG) of wave-propelled unmanned surface vehicles (USVs) rely primarily on the forces exerted by the environment and, for this reason, ensuring an intended navigational behavior at sea is a challenging task. In this article we discuss the design and experimental validation of a gain-scheduled steering control system that governs the course of a wave-propelled USV subject to different sea surface currents. A theoretical investigation of the vehicle nonlinear dynamics identifies in a scalar scheduling variable γ the major source of model nonlinearities due to vehicle's and ocean current velocities. The impact of such nonlinearities on the control of the course-over-ground is investigated with a quasi-linear model analysis in the frequency domain. This provides a basis for the design of a gain-scheduled steering controller, whose theoretical assumptions are supported and validated by extensive simulations and experimental results. Moreover, we show that scheduling of the autopilot gains can still be achieved despite the lack of sea current measurements onboard the USV. Finally, it is demonstrated that the navigation and course-keeping performances improve significantly when the gain-scheduled controller is employed, as compared to the nominal fixed-gain autopilot.

The presented control system is assessed with simulations and validated on a series of field experiences meant to quantify the autopilot robustness and the vehicle course-keeping capabilities.

1. Introduction

The advent of surface and underwater gliders has enabled, in the last decades, a more cost-effective and sustainable way of studying oceanographic phenomena (Smith et al., 2011). One of the main advantages of sea gliders is that, unlike common marine vehicles, they show reduced energy limitations and are, therefore, more suitable platforms to be employed in long-duration missions (Hine et al., 2009; Glenn et al., 2011).

Persistent observation of oceanographic phenomena is necessary in order to understand and anticipate their relatively slow dynamics. In this large picture, marine robotic gliders play a fundamental role which is mainly due to their unique capability of operating for extended period of time, in remote areas and with limited need of human intervention (Camus et al., 2019).

The observation of natural phenomena with long-endurance marine platforms has completely revolutionized ocean studies that, up to few years ago, revolved around ship-based measurements. The limitations of traditional ocean observation methods have become clear when affordable, cost-effective robots have become commercially available and the results have been presented in a number of ocean studies (Ferreira et al., 2018; Costa et al., 2018; McGillivary et al., 2012). Some of the main advantages of employing autonomous marine systems at sea are, for example, that humans are less exposed to harsh environments, scientific missions cost less money and human efforts, CO_2 emissions are reduced and, most of all, natural phenomena are observed at more appropriate spatio-temporal scales.

Despite such glaring advantages, extended autonomy and navigation robustness are hampered by the current technological tools that have struggled to adapt to the new way of conducting ocean studies. For example, when considering surface vehicles propelled by environmental forces, the well-consolidated techniques in the field of control theory need to be adapted as the vehicle's speed and, in some cases the speed-over-ground (SOG) and course-over-ground cannot be governed and a complete loss of maneuverability is observed (Dallolio et al., 2022).

* Corresponding author.
E-mail addresses: alberto.dallolio@ntnu.no (A. Dallolio), henning.overaas@ntnu.no (H. Øveraas), tor.arne.johansen@ntnu.no (T.A. Johansen).

https://doi.org/10.1016/j.oceaneng.2022.111618
Received 19 October 2021; Received in revised form 28 February 2022; Accepted 22 May 2022
Available online 3 June 2022

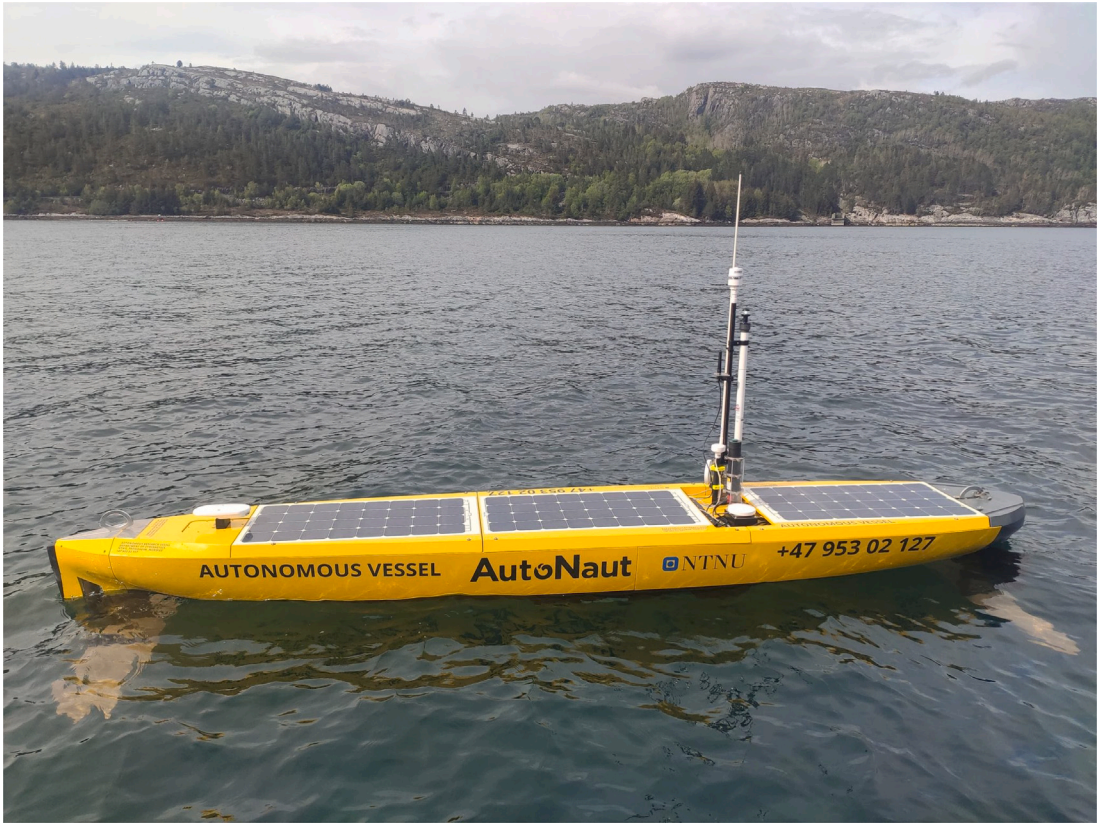

Fig. 1. The NTNU AutoNaut.

These challenges are mainly due to the fact that this unique class of vehicles does not rely on an active propulsion system, but instead on natural propulsion (i.e., waves, currents, winds). As a consequence, navigation systems integrated onboard these vehicles need to be robust enough to cope with different sea states and for extended periods of time (e.g., in the order of weeks). Common navigation and control techniques cannot address the maneuverability limitations due to environmental counteracting forces, as they have been developed assuming the ability of motored propulsion to ensure a minimum speed that is sufficient for maneuverability.

In this article we further extended our previous analysis of a course-keeping control system for the AutoNaut (Dallolio et al., 2022), a commercially available wave-propelled USV (Johnston and Poole, 2017). We employ a version of the AutoNaut (see Fig. 1) in which navigation, communication and payload control systems[1] are designed and developed by the Norwegian University of Science and Technology (NTNU) (Dallolio et al., 2019). As described in Dallolio et al. (2019), the USV is equipped with a wide-range suite of sensors dedicated to different functionalities (i.e., navigation, communication, scientific surveys). In this work, we have mainly focused on the measurements of the global navigation satellite system (GNSS)[2] and of the acoustic Doppler current profiler[3] (ADCP). While the former is used to measure the vehicle's state (location, speed and course over ground, heading), the latter measures velocity and direction of the sea currents relative to the USV.

In our previous work, we have modeled the USV's dynamics and presented control solutions that allow stable course control in different sea states and environmental conditions. In our first investigation, we have identified the main source of model nonlinearity in a parameter named γ, and we have anticipated that this variable can be employed in gain scheduling techniques of the course controller gains. When a controller is designed based on a linearized system, it is guaranteed to work optimally only in some neighborhood of its equilibrium point. However, nonlinear systems may have multiple operating point depending on exogenous disturbances and hence the controller performances may deteriorate (Khalil, 2002). A solution to this is to extend the linearization approach to a range of operating points. This method is called *gain scheduling* and it finds its origins in works related to flight control systems (Rugh and Shamma, 2000). In our work, we identify γ as the *scheduling variable*.

This manuscript brings those assumptions to analysis and validation. In the first part, theoretical considerations are supported with an extensive model analysis in the frequency domain. The authors present two variations of the scheduling approach (with and without ocean current measurement) and demonstrate that the navigation performances are improved in both cases. Feasibility and limitations of both approaches are discussed and supported by simulation and experimental results.

This article is organized as follows. In Section 2 we discuss the principles of gain scheduling and present the three-state quasi-linear model used as a basis for control design. In Section 3 we present the model frequency analysis and the pole placement results for ADCP-based and SOG-based gain scheduling. In Section 4 and Section 5 we present and discuss simulations and experimental results. Conclusions and further considerations are included in Section 6.

2. Theory

2.1. Gain scheduling principles

Gain scheduling is an approach to control of nonlinear systems that makes use of a family of linear controllers (Khalil, 2002). In

[1] http://autonaut.itk.ntnu.no.

[2] Hemisphere V104s GPS Compass: https://www.hemispheregnss.com.

[3] Nortek Signature500: https://www.nortekgroup.com/products/signature-500.

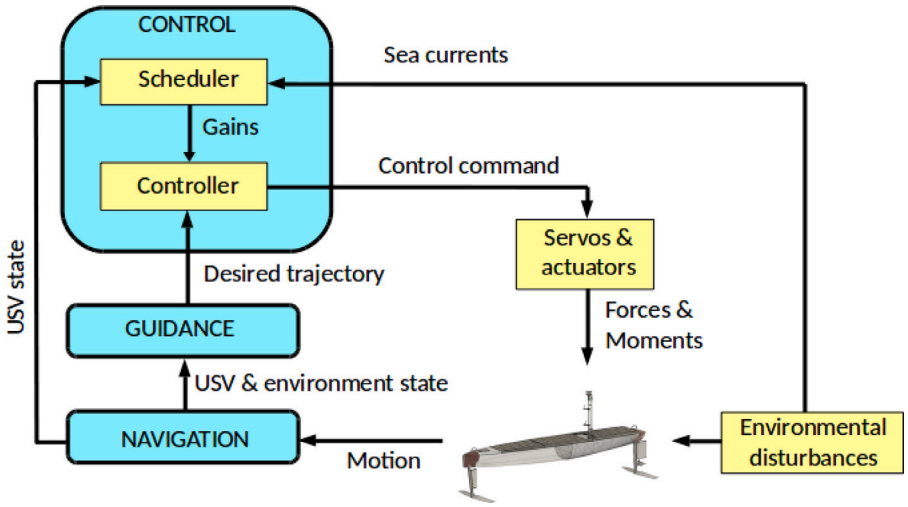

Fig. 2. GNC with gain-scheduled controller.

fact, the single linear controller is meant to provide a satisfactory control performance for its specific operating point of the system. The operating points are characterized by a *scheduling variable*, that is used to adjust the controller gains based on the operating points. Fig. 2 shows a typical guidance, navigation and control (GNC) system with gain-scheduled controller. In this work, the scheduler computes γ (see Eq. (6)) and then adapts the proportional and integral gains that are forwarded to the linear course controller that commands the rudder.
Since each linear controller can be tuned independently, one could see the gain scheduling method as a divide and conquer approach for controlling a nonlinear system where the advantage is that well established linear control theory can be used.

Gain scheduling is a common method which is applied today in a number of fields (Rugh and Shamma, 2000; Leith and Leithead, 2000; Shamma and Athans, 1992). The literature in the field of marine robotics shows several examples in which control strategies make use of gain scheduling. For example, dos Santos and Goncalves (2019) and Santos et al. (2018) demonstrate that gain scheduling can be efficiently employed to tune a low-level heading controller and enhance navigation performances when a sailboat USV navigates into the wind. In Kragelund et al. (2013) classical PID control with gain scheduling is used to adapt the speed of a motored USV. The design of a course control system that makes use of a gain-scheduled PID controller is discussed in Peimin et al. (2018), where the authors have initially identified offline the parameters of a classical Nomoto model (Fossen, 2021). Based on that, they have computed the optimal PID controller parameters using the pole-zero configuration method at different speeds.

In our work, the controller parameters are scheduled using γ, which is a scalar variable defined in (6). Although γ is somewhat influenced by changes in heading and course setpoints, it primarily depends on the longitudinal dynamics of the vehicle that is not much influenced by the course-keeping control between way-points. Hence, it is essentially a slowly time-varying variable, since variations in the sea current and USV's ground speeds are slowly changing processes. This means that the basic time-scale separation principle applies and linear control theory can be safely applied by considering γ as a fixed parameter in the context of gain scheduled control design and stability analysis, Shamma and Athans (1990, 1992). The simulations and experiments presented later confirms the assumption that variations in γ are slow and that there are no stability issue caused by such variations in practice. For completeness, it can be mentioned that there exists numerous methods that can be used to choose controller parameters such that stability can be guaranteed for the nonlinear closed loop dynamics also if γ is assumed to be rapidly time-varying such that the time-scale separation does not hold. Such methods typically rely on the theory of linear parameter-varying (LPV) systems, and use assumptions on the range and rate of γ to design LPV controllers for which a quadratic or quadratic parameter-varying Lyapunov function exists, Shamma and Athans (1991), Apkarian and Gahinet (1995). Such problems can be formulated as convex optimization problems solved using linear matrix inequalities, where the main drawback is that the choice of Lyapunov functions and assumptions on γ are conservative.
The main contribution proposed in this work is the novel and practical gain scheduled control design that is shown, via model analysis and simulations and experimental results, to compensate for the main system nonlinearities when the USV operates at very low speed over ground. Such situations occur when the ocean current and/or wind forces are of the same magnitude as the wave-induced propulsion forces. Unlike other methods, the scheduling process is not a brute force assignment of the gains to pre-computed values, but results instead from the observation of the ocean current velocity and the vessel's velocity over ground. For this reason, the controller is more robust and is able to maintain course-keeping performances in a number of navigation scenarios including different currents, winds and waves.

2.2. Three-state quasi-linear model

Consider the 3-degrees of freedom rigid body and hydrodynamic vehicle model for the horizontal plane (Fossen, 2021)

$$M\dot{\boldsymbol{\nu}}_r + C(\boldsymbol{\nu}_r)\boldsymbol{\nu}_r + D(\boldsymbol{\nu}_r)\boldsymbol{\nu}_r = \boldsymbol{\tau}, \tag{1}$$

where $M = M_A + M_{RB}$ accounts for rigid body and hydrodynamic added mass, $C(\boldsymbol{\nu}_r) = C_A(\boldsymbol{\nu}_r) + C_{RB}(\boldsymbol{\nu}_r)$ accounts for Coriolis and centripetal terms, and $D(\boldsymbol{\nu}_r)$ includes damping terms. In this representation $\boldsymbol{\nu}_r$ is the velocity vector of the vehicle relative to the ocean current: $\boldsymbol{\nu}_r = [u_r, v_r, r]^T$. The vector $\boldsymbol{\tau}$ contains forces in surge and sway, and the corresponding yaw moment, generated by winds, waves, steering and propulsion mechanisms. As described in Dallolio et al. (2022), the Coriolis and centripetal terms depend on the USV's velocity relative to the sea current whose longitudinal and lateral components is defined as: $u_r = u - u_c$ and $v_r = v - v_c$. In vector $\boldsymbol{\nu}_r$, r represents the angular speed in yaw. In this formulation, u_c and v_c are the longitudinal and lateral components of the ocean current velocity vector, respectively, decomposed in the vehicle's BODY coordinate frame,[4] while u and v are the vehicle's BODY-fixed longitudinal and lateral linear velocities.

[4] The current is assumed to be irrotational such that $r_c = 0$.

Moreover, $U = \sqrt{u^2 + v^2}$ and $U_r = \sqrt{u_r^2 + v_r^2}$ are the USV's velocities relative to ground and to the water flow, respectively.
The course angle is defined as the sum of the vehicle's heading (ψ) and the crab angle (β): $\chi = \psi + \beta$. The crab angle is defined as $\beta = \arcsin(v/U)$. Hence, the course angle dynamics can be expressed as

$$\begin{aligned}\dot{\chi} &= r + \frac{1}{1+\frac{v^2}{u^2}}\frac{d}{dt}\left(\frac{v}{u}\right) \\ &= r + \frac{1}{U^2}(\dot{v}u - \dot{u}v).\end{aligned} \tag{2}$$

The expressions for the state dynamics can be obtained by expanding Eq. (1):

$$\dot{v} = -ru_c - \frac{m + A_{11}}{m + A_{22}}u_r r - \frac{D_{22}}{m + A_{22}}v_r + \frac{1}{m + A_{22}}F_Y \tag{3}$$

$$\dot{r} = -\frac{D_{66}}{J_z + A_{66}}r - \frac{A_{22} - A_{11}}{J_z + A_{66}}u_r v_r + \frac{1}{J_z + A_{66}}\tau_Z \tag{4}$$

where m is the mass, A_{11}, A_{22}, A_{66} are hydrodynamic added mass and moment of inertia coefficients, D_{22} and D_{66} are the are linear hydrodynamic damping coefficients, J_z is the moment of inertia about the vertical axis, F_Y and τ_Z are respectively lateral horizontal forces, and yaw moment, generated by the rudder. The wind and waves are not considered explicitly in this analysis, but their effects are implicitly captured through the USV's measured velocity over ground that primarily depends on these forces in addition to the ocean current. We refer to Dallolio et al. (2022) for the full nonlinear rudder model. As described in Dallolio et al. (2022), the assumption of a constant surge velocity u leads to

$$\begin{pmatrix} \dot{\chi} \\ \dot{v}_r \\ \dot{r} \end{pmatrix} = \begin{pmatrix} 0 & -\frac{u}{U^2}\frac{1}{m+A_{22}}(D_{22} + \alpha_{YR}U_r) & \gamma \\ 0 & -\frac{1}{m+A_{22}}(D_{22} + \alpha_{YR}U_r) & -\frac{m+A_{11}}{m+A_{22}}u_r \\ 0 & -\frac{1}{J_z+A_{66}}((A_{22} - A_{11})u_r + \alpha_{ZR}U_r) & -\frac{D_{66}}{J_z+A_{66}} \end{pmatrix} \begin{pmatrix} \chi \\ v_r \\ r \end{pmatrix} + \begin{pmatrix} \frac{u}{U^2}\frac{\alpha_{YR}U_r u_r}{m+A_{22}} \\ \frac{\alpha_{YR}U_r u_r}{m+A_{22}} \\ \frac{\alpha_{ZR}U_r u_r}{J_z+A_{66}} \end{pmatrix}\delta, \tag{5}$$

where α_{YR} and α_{ZR} are constants obtained from a linearization of the steering model, and δ is the rudder angle. Eq. (5) allows us to isolate the main source of nonlinearity in the variable named γ:

$$\gamma = 1 - \frac{u}{U^2}u_c - \frac{u}{U^2}\frac{m + A_{11}}{m + A_{22}}u_r. \tag{6}$$

In the following section we use the three-state model of Eq. (5) for gain-scheduled control design. We denote: $H_{ql}(s) = \frac{\chi}{\delta}(s)$ the transfer function of the presented quasi-linear model; $H_{ql}(s)/\gamma$ the normalized transfer function; $C_{pi}(s)H_{ql}(s)$ and $C_{gs}(s)H_{ql}(s)$ transfer functions of the open-loop systems with fixed-gains PI and gain-scheduled controllers, respectively; $M_{pi}(s) = C_{pi}(s)H_{ql}(s)/(1 + C_{pi}(s)H_{ql}(s))$ and $M_{gs}(s) = C_{gs}(s)H_{ql}(s)/(1 + C_{gs}(s)H_{ql}(s))$ the complementary sensitivity functions of the two closed-loop systems; $N_{pi}(s) = 1/(1+C_{pi}(s)H_{ql}(s))$ and $N_{gs}(s) = 1/(1 + C_{gs}(s)H_{ql}(s))$ the corresponding sensitivity functions.

3. Methods

In Dallolio et al. (2022) it is shown that the main variations in dynamics are due to the parameter γ that influences the gain in the simplified Nomoto model. The frequency analysis confirms that course-keeping control should therefore consider the variations in the gain γ, and use that knowledge to counteract the disturbances due to winds, waves and current. Much can be achieved with the integral action, since the current, wind and wave-driven propulsion speeds can be expected to be slowly time-varying variables. Moreover, while the integral action is well suited to handle additive disturbances, it is not sufficient to handle multiplicative disturbances (as the factor γ). Gain scheduling based on γ is therefore an interesting approach, and the design of a gain-scheduled course controller is justified by the fact that the main nonlinearities are introduced by the slowly time-varying environmental parameters (winds, waves and current) as well as the course angle command.

3.1. Model frequency analysis

Fig. 3 shows the values of γ when considering a range of typical longitudinal AutoNaut's speed and ocean current values, e.g., $u \in [0, 1.5]$ m/s and $u_c \in [-1, 1]$ m/s. As discussed in our previous work (Dallolio et al., 2022), singularities are reached when the vehicle's ground speed drops towards zero in presence of ocean currents. Far from singularities, γ stabilizes around the nominal values $\gamma^n = 0.4$, which is the value that γ reaches when the current u_c is zero and when no lateral motion is observed (i.e., $U = u$), as shown in Fig. 3. Further analysis reveals that γ becomes negative when $u_c \geq u$, i.e., $u_r \leq 0$. From a control perspective this would lead to gain sign changes which means that the vehicle is "driving in reverse", which is not a desirable situation. In the transition from positive to negative gain, there is a singular uncontrollable state when $u_r = 0$, where the rudder has no effect. In this analysis we therefore assume $u_r > 0$ and hence $\gamma > 0$. This means that the analysis excludes situations in which $u_c > u$ in the USV's BODY frame, i.e, when the vehicle is transported "in reverse" by a current and its speed is lower than that of the current itself.

Fig. 4 shows the frequency response (Bode plot) of the quasi-linear model for a set of different values of u_r. The relative longitudinal speed u_r is computed assuming a fixed longitudinal speed of the USV $u = 0.8$ m/s and a varying current $u_c \in [-0.7, 0.7]$ m/s in BODY frame. As u_r varies, the major differences are in the magnitude of the gain (≈ 85 dB), although some phase variations are also observed. While increased gain is observed for high relative velocities, lower relative velocities reduce the system bandwidth to lower frequencies, i.e., at low u_r the rudder response is slower when trying to control the USV's course. In order to better evaluate the impact of γ, the quasi-linear system is normalized as shown in Fig. 5. Since γ appears as a gain in the transfer function, no change in phase variations are expected. It can however be observed that gain variations are significantly reduced to ≈ 15 dB. Notably, the gain variations are smallest for $0.1 \text{ rad/s} \leq \omega \leq 0.4$ rad/s, where the closed loop control bandwidth may be located. In fact, control design models should have smallest uncertainty in this frequency range since this will lead to best stability margins. This suggests that most of the model variation due to changes in u_r are captured by γ, and further suggests this variable may be suitable for gains scheduling. Based on this, we propose that the system can be controlled by a PI controller with a simple gain scheduling with the factor $1/\gamma$:

$$C_{gs}(s) = \frac{1}{\gamma}C_{pi}(s) = \frac{K_p}{\gamma}\left(1 + \frac{1}{T_i s}\right), \tag{7}$$

where K_p is the proportional gain and T_i the integration time.

The linearized closed-loop stability properties can be investigated by analyzing the phase and gain margins of the open-loop system. Figs. 6 and 7 show the Bode plots of the open-loop transfer functions $C_{pi}(s)H_{ql}(s)$ and $C_{gs}(s)H_{ql}(s)$ respectively, where a lower bound on γ ($\gamma \geq 0.05$) was used in order to avoid it becoming infinitely small (and hence the gains infinitely large). Fig. 6 shows that when the fixed-gain linear controller is employed it is hard to find a set of gains which both achieve high control bandwidth and make the closed-loop systems stable for all values of u_r due to the large variation in the gain. The variation in the cross-over frequency is very large, i.e., when u_r is low the system is very slow and when it is high the system is very fast. The difference in cross-over frequency between the lowest and higher u_r spans almost four orders of magnitude, and at high values of u_r the system is unstable. Stability margins are also weak at low u_r values. Since the course dynamics acts as a pure integrator, including the integral action also in the controller would result in low phase margins unless the integral gain are chosen to be very small. Despite

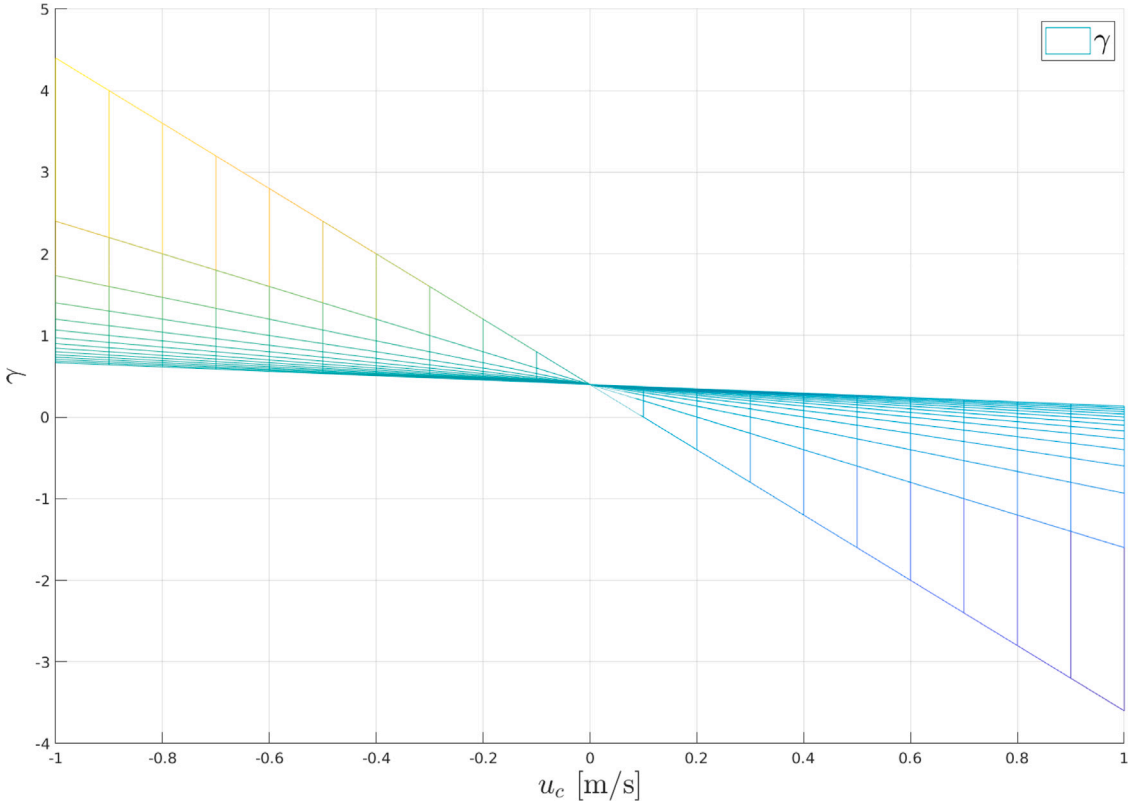

Fig. 3. Nominal value $\gamma^n = 0.4$.

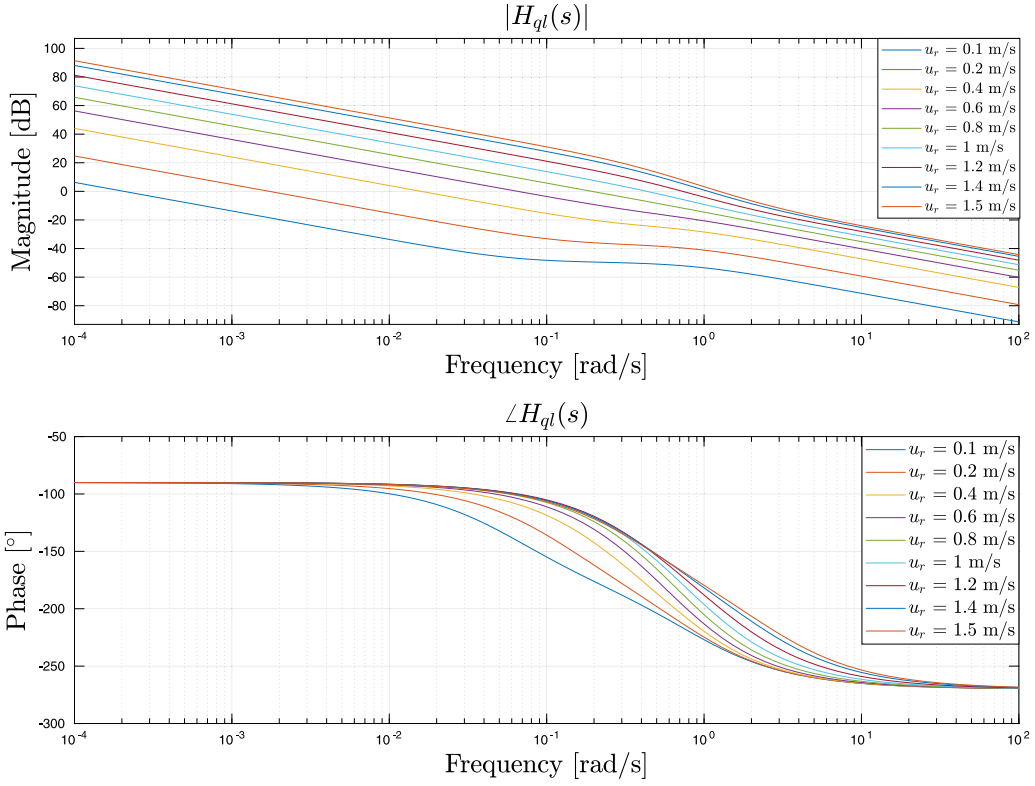

Fig. 4. Magnitude (top) and phase (bottom) of H_{ql}.

derivative action in the controller may improve the stability margins, this option is discarded for reasons described below.

Fig. 7 shows that when the gain-scheduled controller is included in the open-loop the gain variations decrease and the bandwidth of the

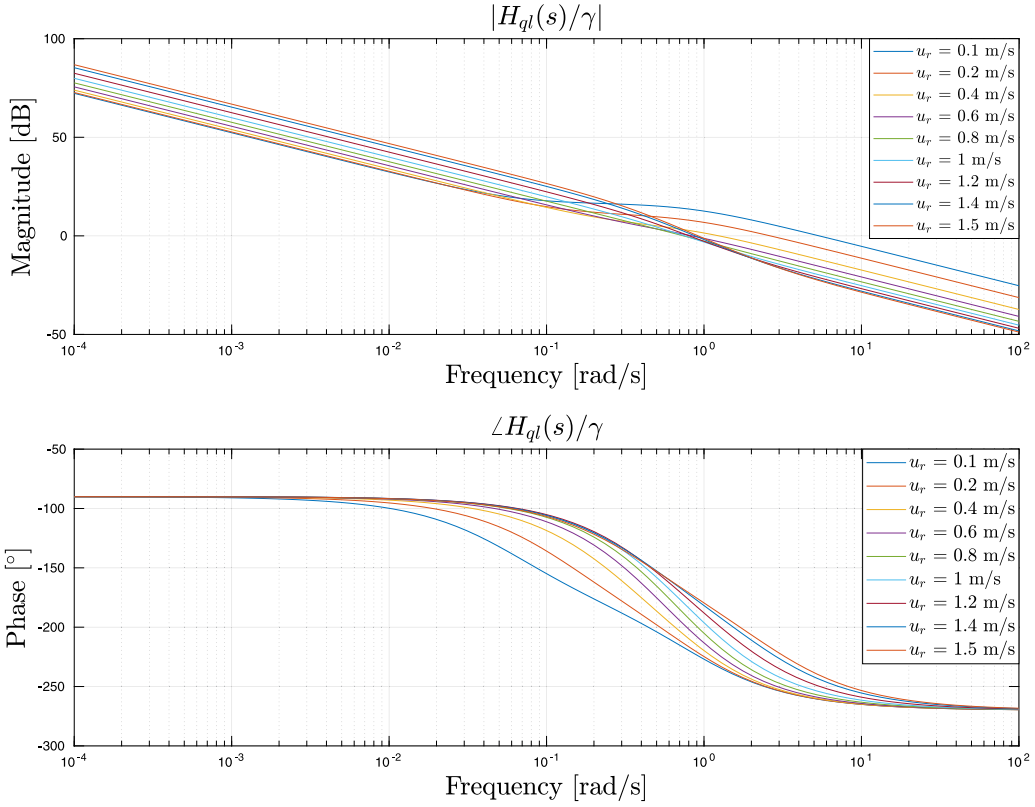

Fig. 5. Magnitude (top) and phase (bottom) of H_{ql}/γ.

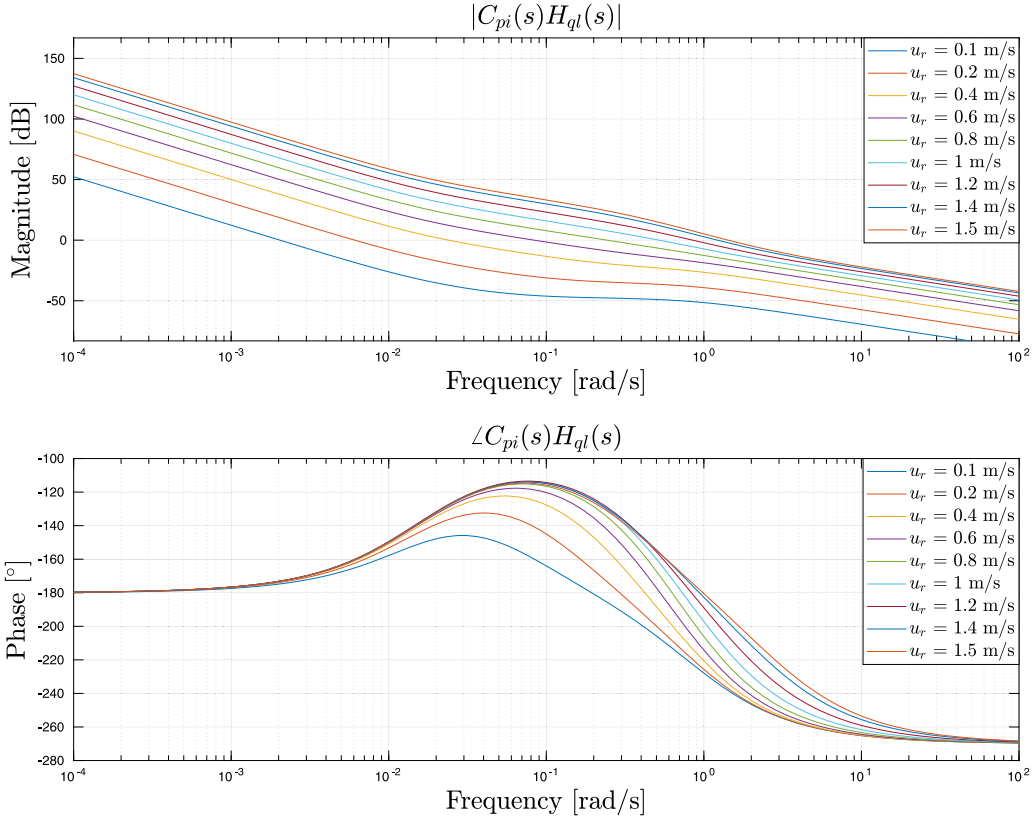

Fig. 6. Magnitude (top) and phase (bottom) of the open-loop system $C_{pi}H_{ql}$ (fixed-gain).

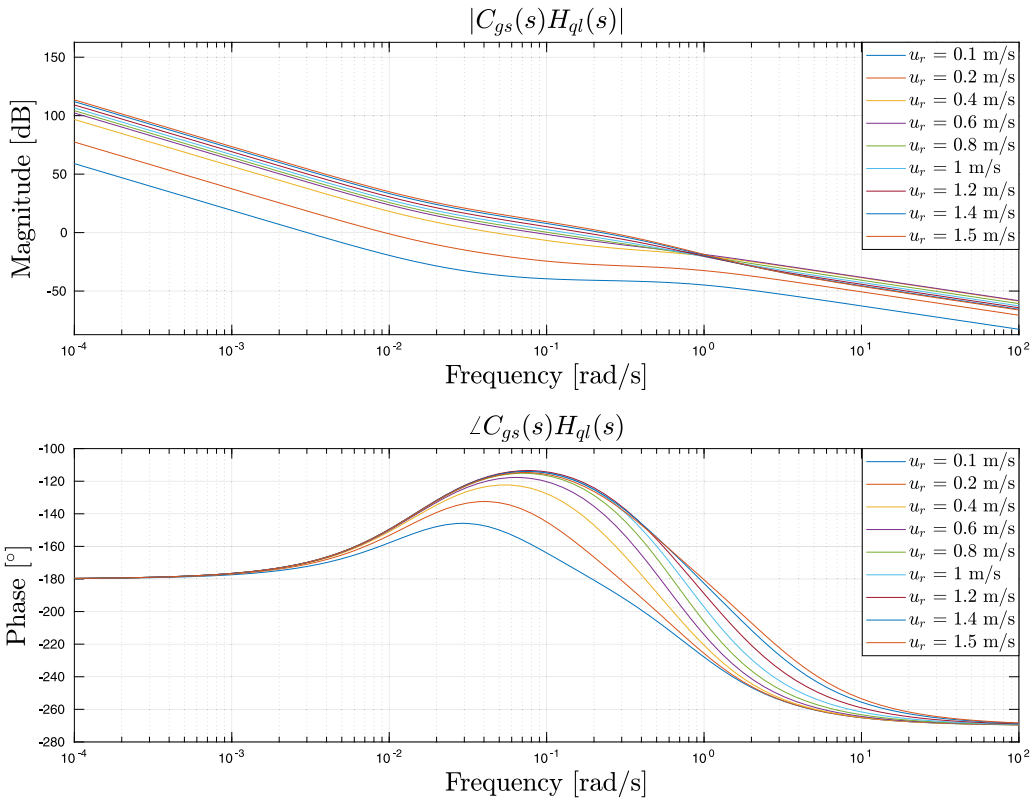

Fig. 7. Magnitude (top) and phase (bottom) of the open-loop system $C_{gs}H_{ql}$ (gain scheduling).

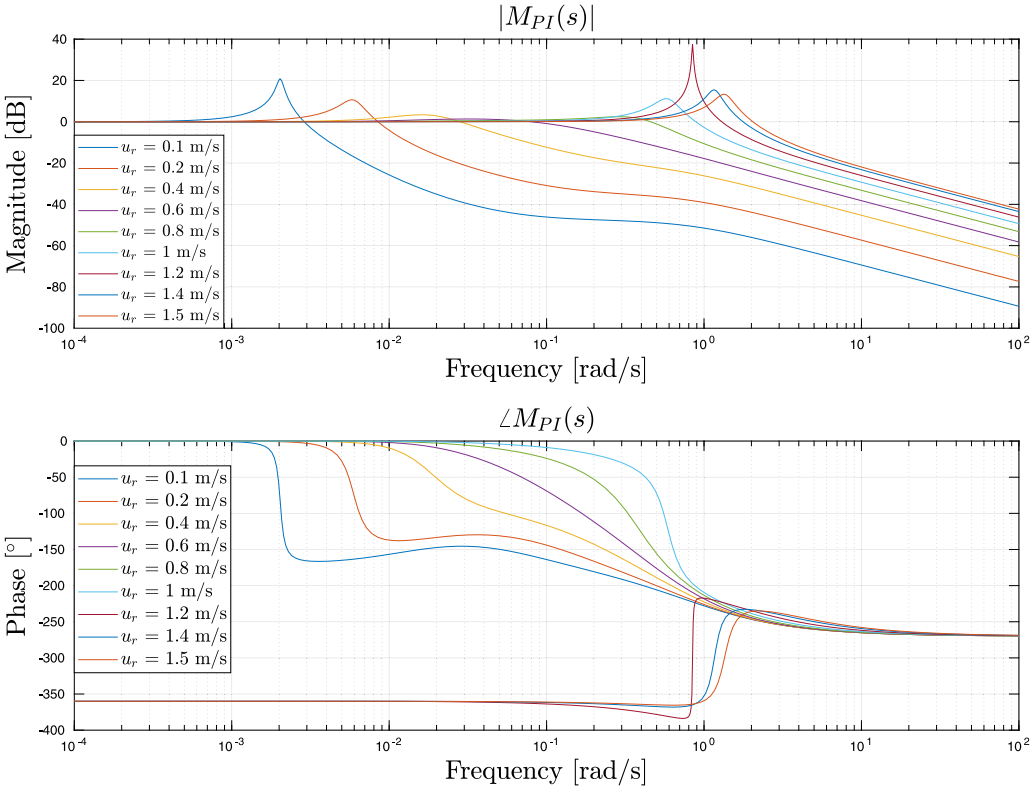

Fig. 8. Magnitude (top) and phase (bottom) of the complementary sensitivity function M_{pi}.

family of transfer functions narrows down mostly to the range between 0.01 rad/s and 1 rad/s. In other words, it is possible to find a combination of gains that make the closed-loop system stable for each value of the considered relative velocity.

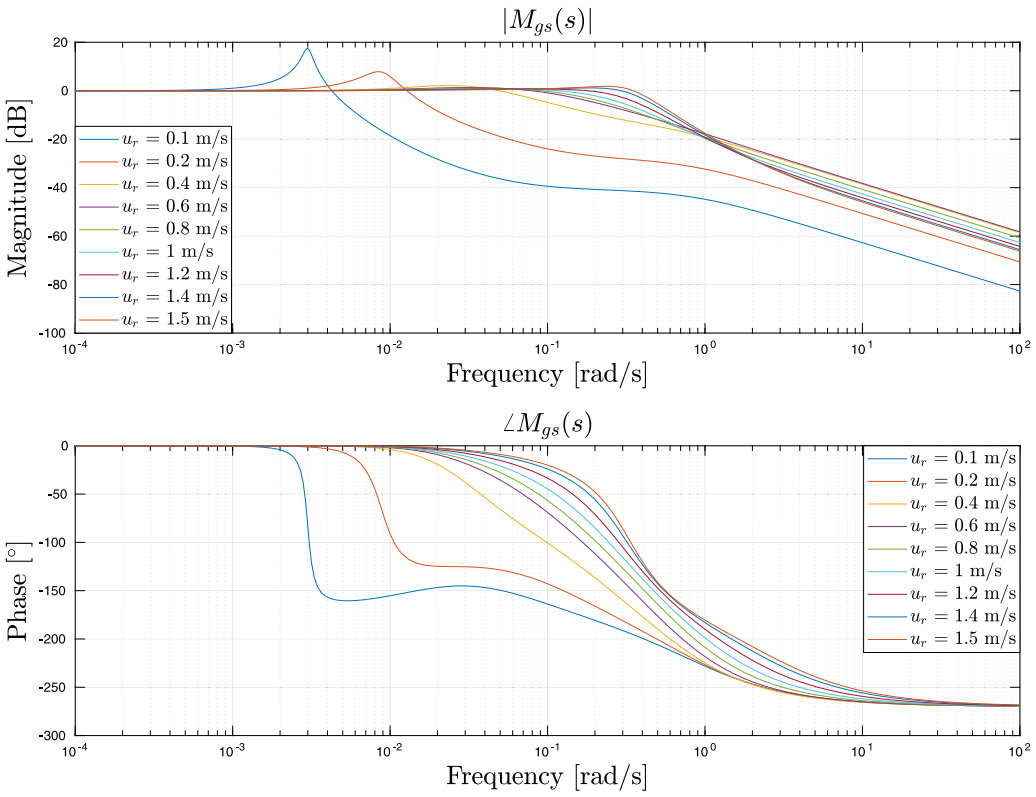

Fig. 9. Magnitude (top) and phase (bottom) of the complementary sensitivity function M_{gs}.

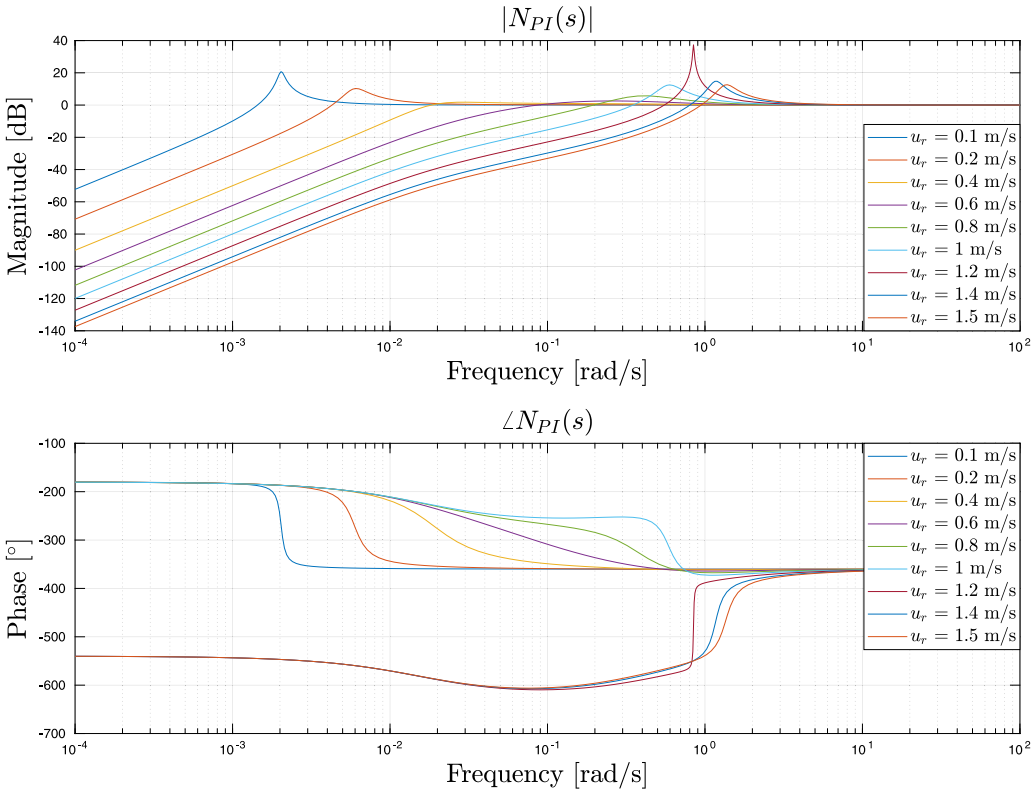

Fig. 10. Magnitude (top) and phase (bottom) of the sensitivity function N_{pi}.

Figs. 8 and 9 show the Bode plots of the complementary sensitivity functions M_{pi} and M_{gs}, used to evaluate the systems' ability to track the reference. For low relative velocities the bandwidth is reduced (see Fig. 8), meaning that the controller is only able to track course references of very low frequency. Also the gain-scheduled controller will have troubles tracking the course reference when the relative velocity

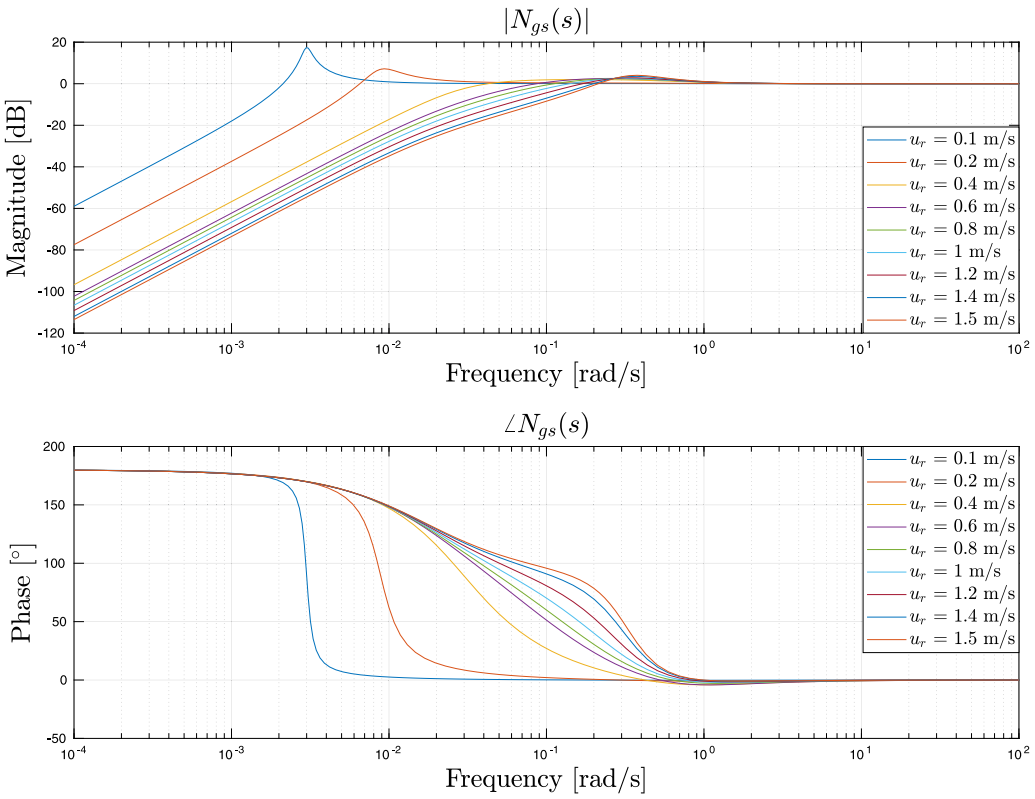

Fig. 11. Magnitude (top) and phase (bottom) of the sensitivity function N_{gs}.

is low, as the bandwidth is smaller than the expected frequencies of the course reference (see Fig. 9). This may justify a different control strategy for very low relative velocities, e.g., heading control (Dallolio et al., 2022). For the linear controller, the closed-loop system becomes unstable for high relative velocities ($u_r \geq 1.2$ m/s), and explains the unusual phase of these systems.

Fig. 9 shows that, for large relative velocities, the gain-scheduled controller has significantly better tracking properties compared to the fixed-gain one.

Figs. 10 and 11 show the Bode plots of the sensitivity functions N_{pi} and N_{gs}, which are used to evaluate the systems' ability to reject noise and disturbances. The magnitude of the sensitivity plots shows the frequencies that are rejected or amplified in the closed-loop system. It can be noticed that the magnitude peaks for some of the considered relative velocities with the PI controller are large (see Fig. 10). The three largest peaks (up to 38 dB) correspond to the cases where the system is unstable, and any noise or disturbances with frequency corresponding to one of the peaks will be amplified by the closed-loop system. For the linear controller with fixed gains (see Fig. 10) at $u_r = 0.1$ m/s the peak is at 0.6 rad/s (period of approximately 10 s). This falls within typical frequencies of ocean waves and it is therefore important that the controller is robust enough to reject them from the closed-loop system. This technique is named *wave filtering* and the importance of attenuating wave-induced first-order oscillatory components in the rudder is more investigated in Dallolio et al. (2021).

Fig. 11 shows that when the gain-scheduled controller is employed the peaks are smaller, meaning that the closed-loop system will amplify the disturbances less. Moreover, the peaks are located around 0.4 rad/s, corresponding to a period of 15 s, which is larger than the most commonly encountered wave periods. This indicates that using derivative action in the controller, as discussed earlier, is not beneficial as the increased controller bandwidth would increase sensitivity to first-order wave disturbances.

3.2. Scheduling of the course controller gains

By selecting the gains according to γ, the control system will ensure stable course control when either the USV's ground speed (U) or its longitudinal velocity relative to water (u_r) become small. The controller gains are computed according to

$$K_p = \frac{\gamma^n}{\gamma} K_p^n \tag{8}$$

$$K_i = \frac{\gamma^n}{\gamma} K_i^n, \tag{9}$$

where γ^n is the nominal value and K_p^n and K_i^n are nominal gain values defined according to Dallolio et al. (2022).

As already discussed in Dallolio et al. (2022), the practical realization of a gain-scheduling strategy is mostly hampered by physical limitations of the onboard ADCP instrument.

In the following we present and discuss two approaches in which γ is computed based on the available information.

3.2.1. ADCP-based gain scheduling

If the ADCP instrument is available, the longitudinal current u_c can be computed as described in Appendix. This means that we can compute γ according to Eq. (6).

In this analysis we consider for simplicity that the current in the USV's BODY frame has no lateral component, i.e., $v_c = 0$ and we compare the stability of two closed-loop systems: one controlled with a fixed-gain PI controller and the other with a gain-scheduled PI controller. The model used in this analysis is the one in Eq. (5), while the nominal controller gains are the same as in Dallolio et al. (2022): $K_p^n = 1.25$ and $K_i^n = 0.02$. In this scenario, the USV travels at a ground speed $U = u = 0.54$ m/s that corresponds to 1 knot, a typical speed for the AutoNaut. In this situation, we simulate and analyze the closed-loop stability when the vehicle is also affected by a current $u_c \in [-1, 0.5]$ m/s. Fig. 12 shows the poles of the closed-loop systems with respect to the relative speed U_r. In the first plot (top), we observe that the higher the relative speed,

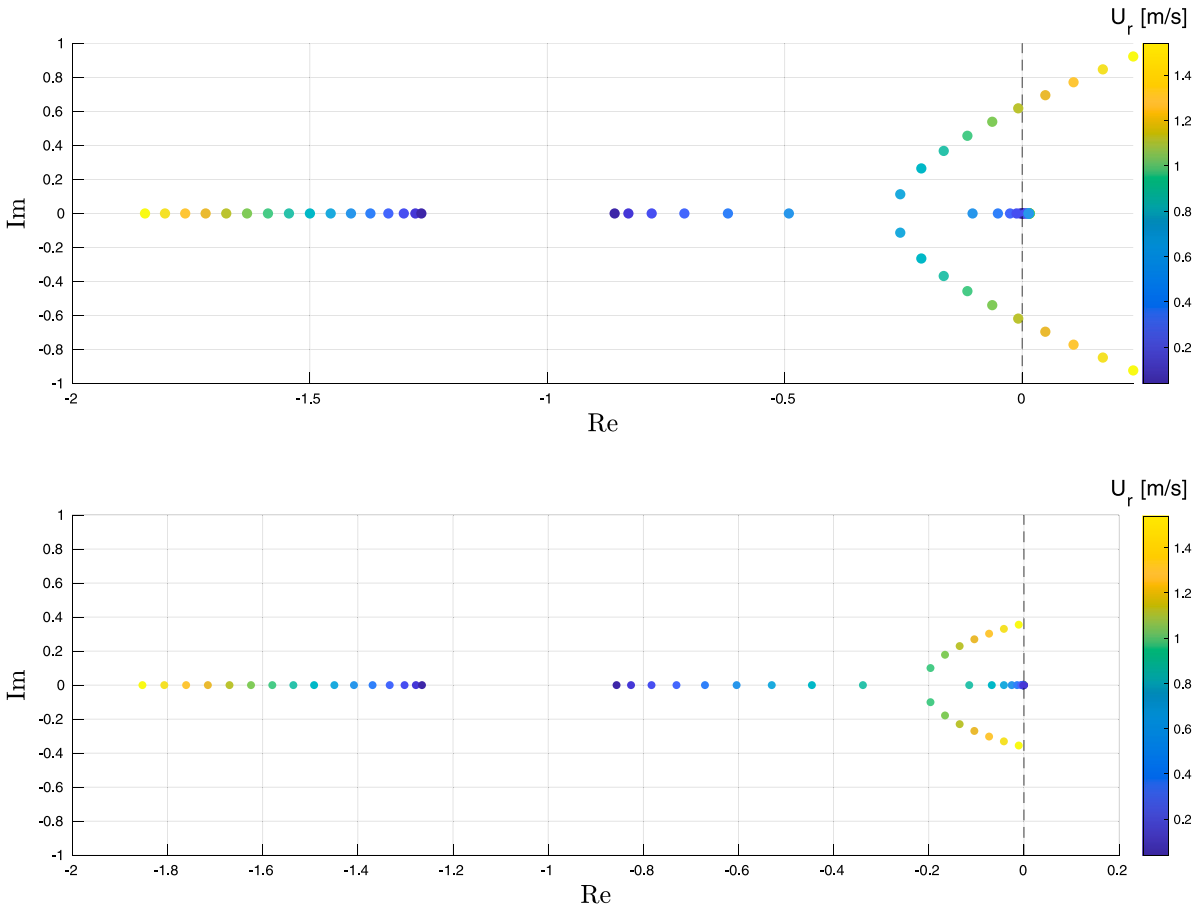

Fig. 12. Closed-loop poles for the fixed-gain course controller (top); closed-loop poles for the gain-scheduled course controller (bottom).

the more unstable the system is, meaning that the controller is not able to maintain stability in the system with the fixed gains. On the other hand, gain scheduling based on the parameter γ allows the closed-loop system to remain stable (poles in the left half-plane) even when the relative speed increases, as shown in the bottom graph.

Despite it is impossible to associate the poles to the system states (χ, v_r, r), the pole placement analysis indicates if the closed-loop system is stable or unstable with the employed PI controller. For the purpose of course-keeping, it is useful to confirm that the closed-loop system is stable with the chosen gains.

3.2.2. SOG-based gain scheduling

The nonlinearities introduced by γ are mainly caused by of the vehicle's ground speed relative to the speed of ocean currents (i.e., U_r). In circumstances in which the sea current cannot be measured, the gains of the course controller can still be adapted assuming knowledge of the USV's ground speed U and longitudinal speed u:

$$\gamma_U \approx 1 - \frac{u^2}{U^2}\frac{m + A_{11}}{m + A_{22}}. \tag{10}$$

However, Eq. (10) reduces to $\gamma = 0.4$ when $v = 0$ m/s. This means that in order to schedule the controller gains, the lateral velocity component is essential.

We assume therefore that the current is not measured and that the USV's speed in the BODY frame is made of a longitudinal and lateral component. In this scenario, the USV travels with a ground speed U that varies from 0 m/s to 1 m/s and again to 0 m/s. Fig. 13 shows the results of the pole placement analysis. It can be observed that when the USV's ground speed drops towards zero, the closed-loop system with the fixed-gain controller becomes unstable and the poles reach the right half-plane. Again, the gain-scheduled controller manages to keep the system stability.

Table 1
Simulation parameters.

	Symbol	Value (Exp. 1)	Value (Exp. 2)
Initial location	L^{init}	(0,0) m	(0,0) m
Initial long. speed	u^{init}	0.35 m/s	0.2 m/s
Initial COG	χ^{init}	0°	0°
Desired COG	χ_d	0°	[0,90,180]°
WP location	WP	(0,75) m	[(0,75),(50,75),(50,0)] m
Current dir.	β_c	180°	−45°
Current speed	U_c	0.3 m/s	[0,0.3] m/s

4. Simulation results

The proposed gain scheduling technique is initially tested in simulation. The full nonlinear model of Eqs. (2)–(4) is implemented in the MATLAB®/Simulink environment. Closed-loop simulations are achieved by simulating a line-of-sight (LOS) guidance system that computes desired vehicle courses from a list of way points. On the basis on the quasi-linear model of Eq. (5), we compared the response of two USVs with the same nonlinear dynamics but with different course controllers. Whereas the course of one USV is controlled by a fixed-gain PI controller with nominal gains K_p^n and K_i^n, the gains of the other are computed according to Eq. (9). Table 1 contains the parameters that were used in the two simulations presented below.

4.1. Straight line navigation with environmental disturbance

In the first simulation the USV navigates North ($\chi_d = 0°$) with initial speed $U = u^{init} = 0.35$ m/s. At time $t = 400$ s a current from North to South appears (direction in Earth-fixed coordinates $\beta_c = 180°$)

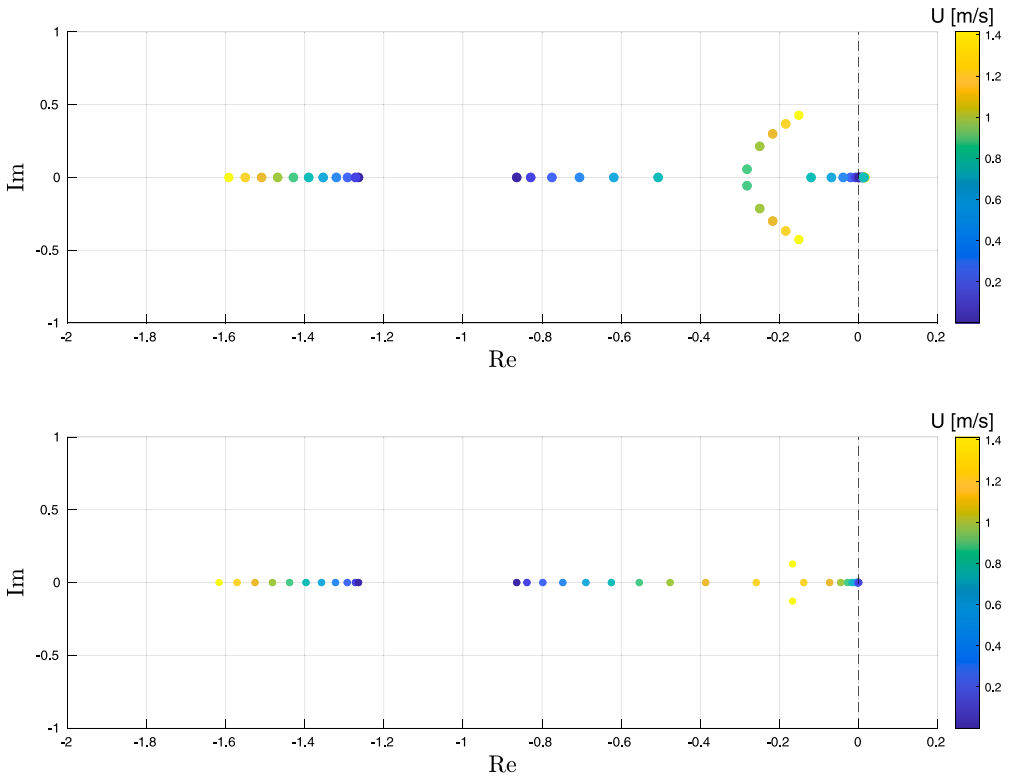

Fig. 13. Closed-loop poles for the fixed-gain course controller (top); closed-loop poles for the gain-scheduled course controller (bottom).

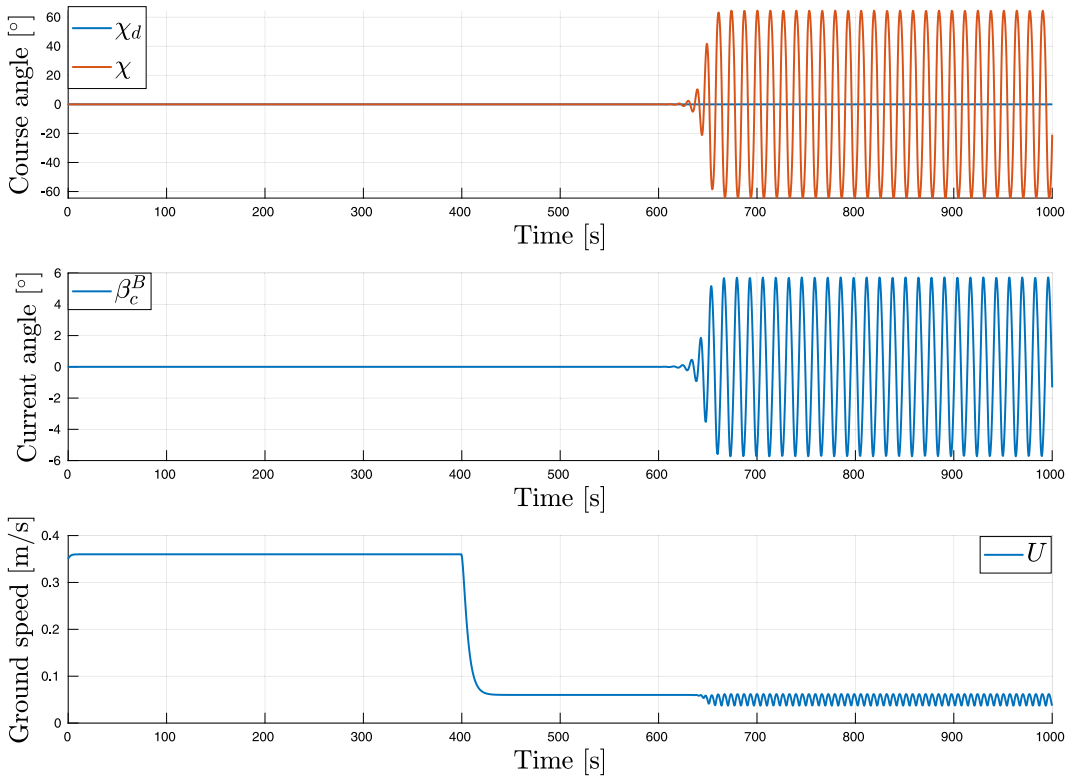

Fig. 14. Desired (χ_d) and measured (χ) course over ground (top); ocean current direction (β_c^B) in vehicle's BODY frame (middle); vehicle's ground speed (U, bottom).

with total speed $U_c = 0.3$ m/s. Fig. 14 compares the desired (χ_d) and measured (χ) course over ground of the vehicle controlled with fixed (nominal) gains $K_p^n = 1.25$ and $K_i^n = 0.02$. It can be observed that when the current hits the vehicle its ground speed decreases below 0.1 m/s (bottom plot). The USV's course is not initially affected by the sea currents, but as the ground speed keeps decreasing slowly and drops below 0.06 m/s oscillations appear. Fig. 14 shows that course oscillations reach 60° of amplitude, therefore proving the inability of the controller

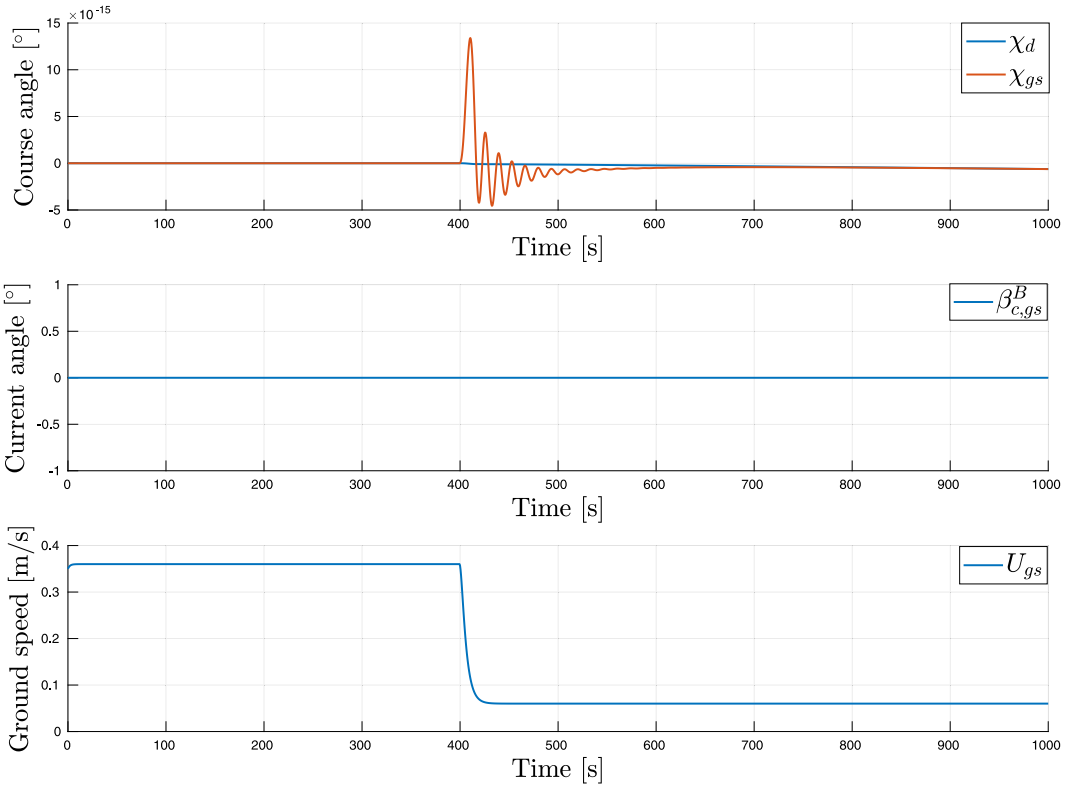

Fig. 15. Desired (χ_d) and measured (χ_{gs}) course over ground (top); ocean current direction ($\beta^B_{c,gs}$) in vehicle's BODY frame (middle); vehicle's ground speed (U_{gs}, bottom).

to maintain a stable course control. The vehicle controlled with a gain-scheduled PI controller manages instead to keep a stable course despite the ocean current, as shown in Fig. 15. This figure clearly indicates that adapting the gains according to the observed ocean current allows the USV to maintain the intended course and navigate more efficiently towards the desired location. Fig. 16 also shows the adaptation of gains according to γ. The top graph compares the value of γ computed during the simulation to its nominal value $\gamma^n = 0.4$. Fig. 16 also shows the relaxation of controller gains needed to cope with the speed drop. The last graph of the same figure compares the rudder angle commanded by the course-keeping autopilot of both vehicles. Whereas the fixed-gain controller commands large rudder efforts, reaching saturation, the rudder compensation commanded by the gain-scheduled controller are small enough to be considered negligible.

4.2. Way points navigation with environmental disturbance

In this simulation we observe and compare the USVs responses during turns and we increase the difference between the initial speed of the vehicles and the ocean current velocity. Table 1 shows the initial USV state, the location of the way points and the desired courses computed by the guidance system each time a way point is reached (Exp. 2 column). Both vehicles are initially moving North with ground speed $U = u^{init} = 0.2$ m/s when at time $t_1 = 300$ s a current directed towards North-West ($\beta_c = -45°$) appears with speed $U_c = 0.3$ m/s. The current fades away at time $t_2 = 1500$ s. Figs. 17 and 18 show the steering response of both vehicles. Fig. 17 shows that the USV controlled with fixed gains is not able to cope with the speed drop and its course starts oscillating around the desired one. In Fig. 18 we notice instead that the system controlled with gain scheduling robustly governs the course over ground, avoiding propagation of the rudder and course oscillations. The current appears while the vehicles navigate between the first and second way points (see Fig. 20). While the course of the USV governed by fixed-gains controller starts oscillating and drifting North, the vehicle with gain-scheduled course control efficiently reaches the second way point (WP 2) and then aims towards the third (WP 3). Some initial oscillations are observed when the current appears and when the way point is reached (see Fig. 18). Fig. 19 indicates that scheduling the gains based on the value of γ helps damping rudder and course oscillations. The impact of currents on the vehicles navigation is best observed in Fig. 20, where it is clear that the ocean current transports both USVs North. The impact of drifting forces generated by the current on the USV navigation can be noticed while the system with gain-scheduled steering control navigates between WP 2 and WP 3. Finally, when the sea current disappears, both vehicles resume normal navigation with nominal gains. The simulation terminates when one vehicle reaches the initial location. The USV with gain-scheduled control navigates more efficiently, hence reaching the destination while the other is still far behind.

5. Field experiments

The USV is equipped with a Nortek Signature500 ADCP with four tilted beams that sample the water column as represented in the Appendix Fig. 29. The instrument measures current components in the beam frame (see Fig. 29) up to a depth of 60 m. The ADCP is in general a very complex instrument, whose performances can vary significantly depending on the application. Factors such as bathymetry, flow turbulence and suspended matter may influence the stream velocity measurements and, to date, a rigorous assessment of ADCP measurement uncertainty is not yet available. The mean velocity spatial distribution is therefore subject to uncertainty associated with ping ADCP errors and the fact that instantaneous measurements both represent the mean velocity and turbulent velocity fluctuations. This means that instantaneous raw data are affected by variance due to both measurement error and real fluctuations and, therefore, instantaneous measurement may be a poor realization of the local mean velocity in some occasions (Kim and Yu, 2010). The experimental results presented in this article are based on sea trials conducted in the Trondheim Fjord at outlet of the Nidelva river (see Fig. 21). Tidal currents can be very

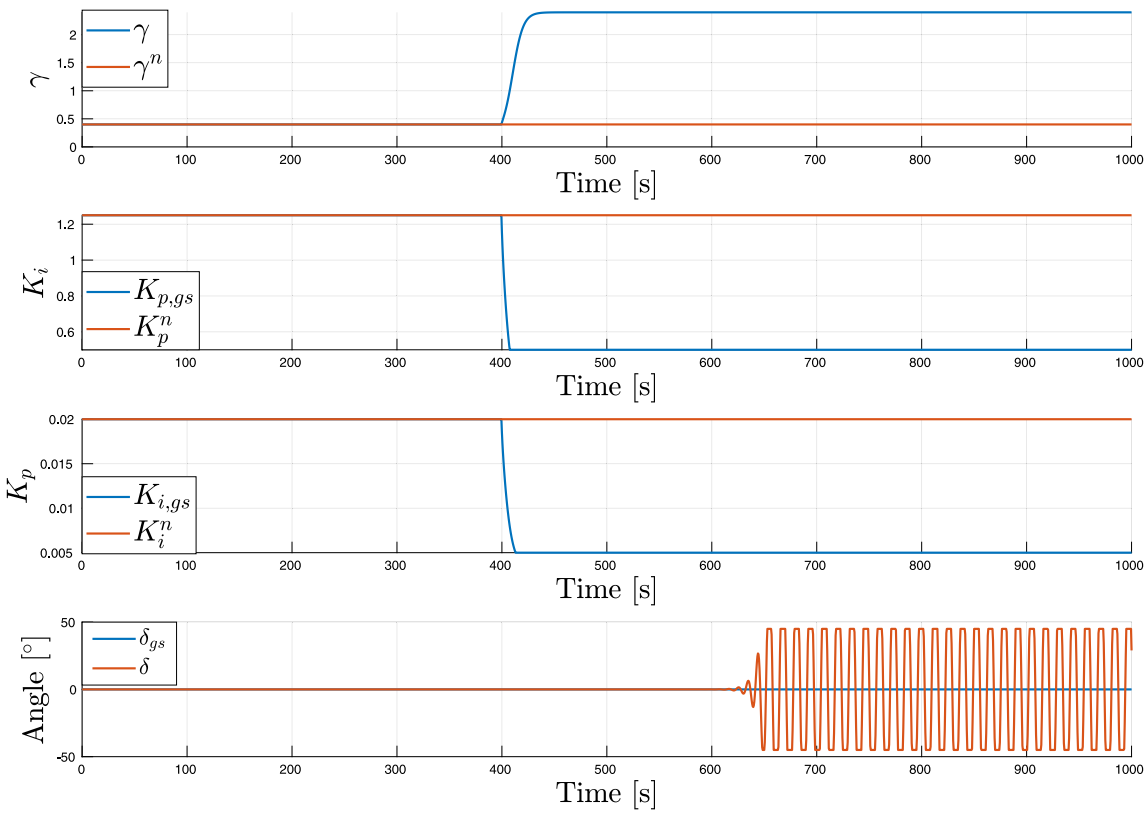

Fig. 16. γ parameter for gain scheduling as compared to its nominal value (γ^n); computed $K_{p,gs}$ and $K_{i,gs}$ gain as compared to their nominal values K_p^n and K_i^n (middle); comparison of the scheduled (δ_{gs}) and not (δ) rudder angles.

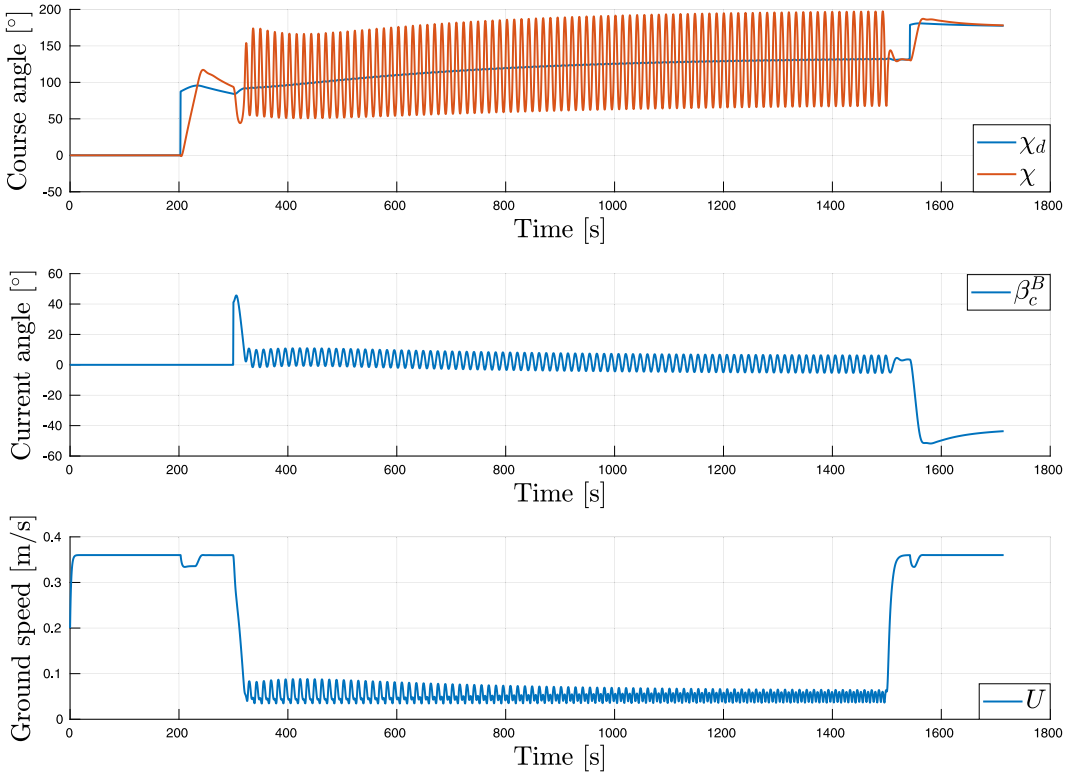

Fig. 17. Desired (χ_d) and measured (χ) course over ground (top); ocean current direction (β_c^B) in vehicle's BODY frame (middle); vehicle's ground speed (U, bottom).

strong in fjords, depending on their width, depth and other factors. As described in Dallolio et al. (2022), there are situations in which the forces generated by the environment overcome the wave propulsion force. The area north of Munkholmen island is known for its strong

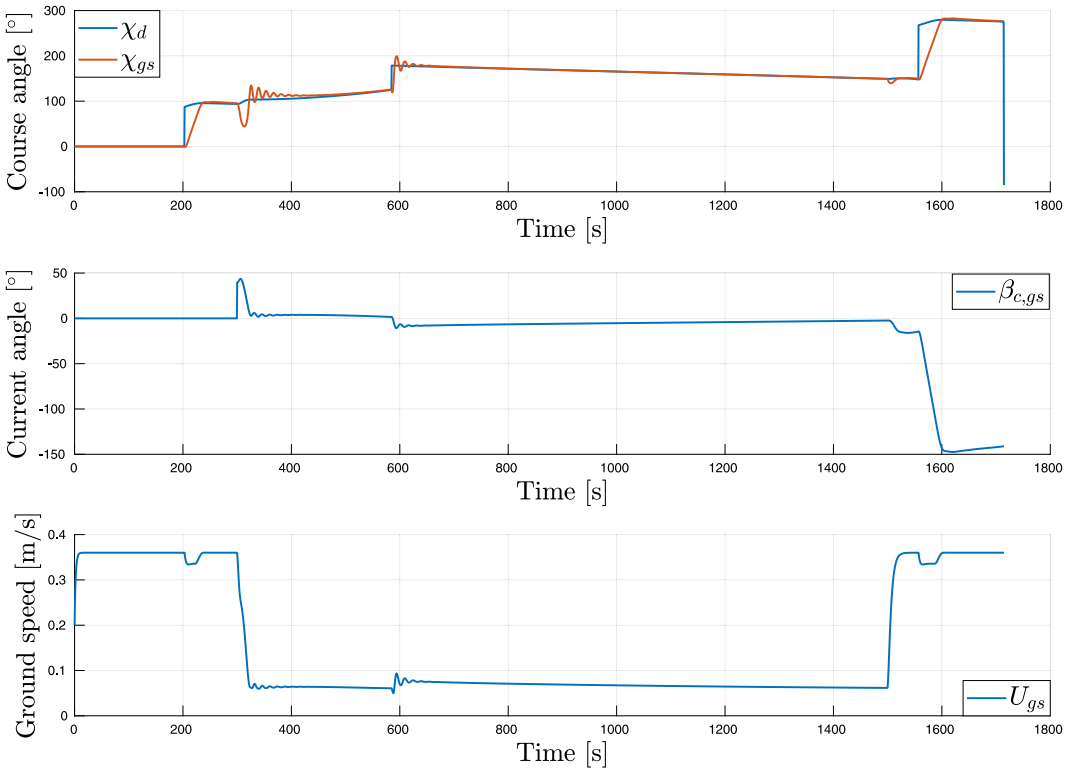

Fig. 18. Desired (χ_d) and measured (χ_{gs}) course over ground (top); ocean current direction ($\beta^B_{c,gs}$) in vehicle's BODY frame (middle); vehicle's ground speed (U_{gs}, bottom).

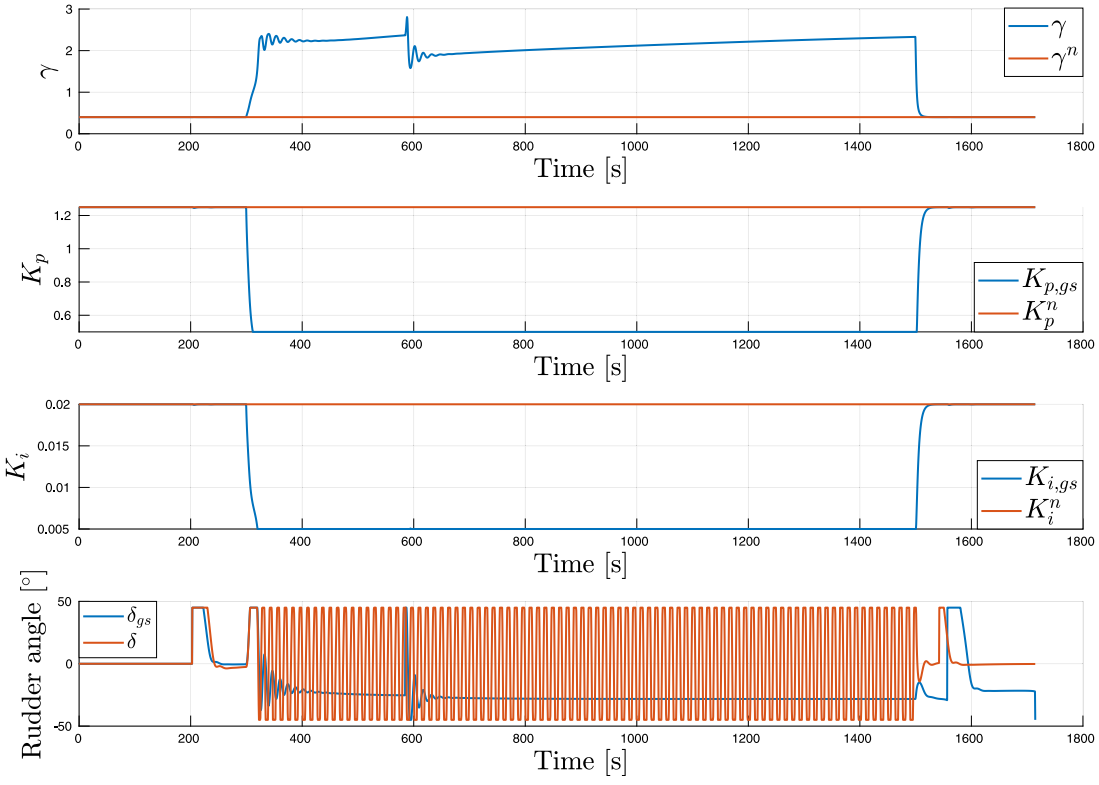

Fig. 19. γ parameter for gain scheduling as compared to its nominal value (γ^n); computed $K_{p,gs}$ and $K_{i,gs}$ gain as compared to their nominal values K_p^n and K_i^n (middle); comparison of the scheduled (δ_{gs}) and not (δ) rudder angles.

currents, due to the steepness of the island shelf. For this reason, on the day of the mission it was decided to conduct the test close to the river outlet. The benefits of operating in this area are two. First, the vehicle can experience a constant current (river outflow) and hence it is easier to test the controller methodically. Secondly, we are able to assess the accuracy of the ADCP measurements, important for the gain

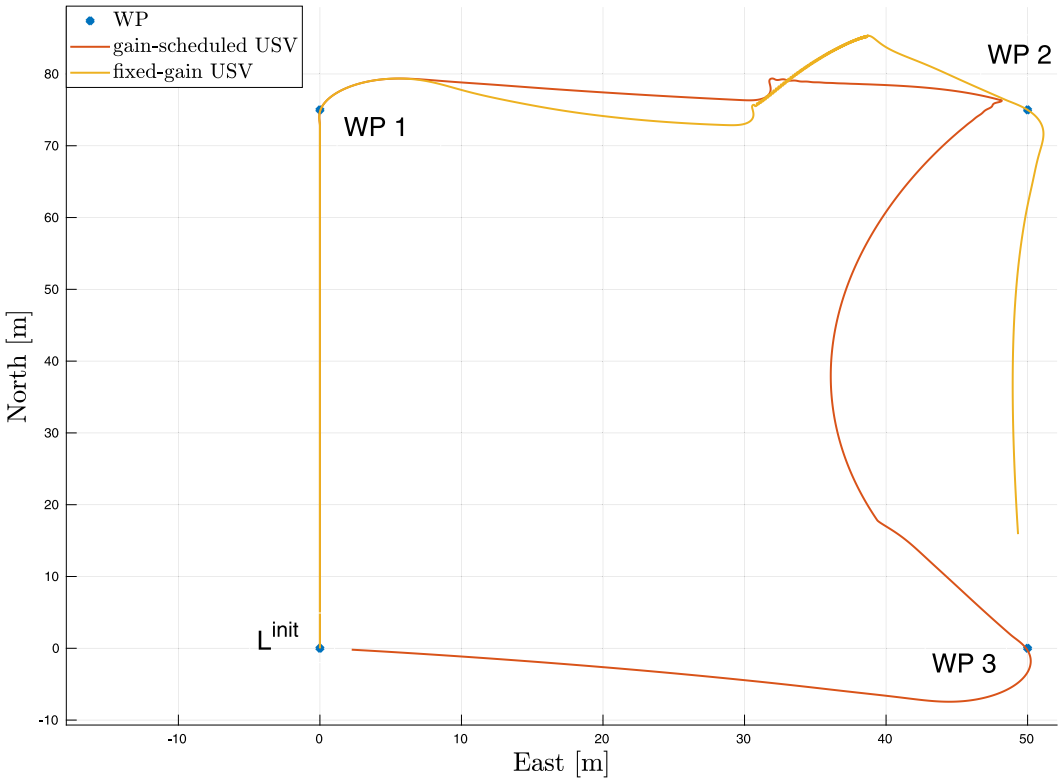

Fig. 20. Vehicles' path.

scheduling procedure. Additionally, proximity to the deployment and recovery facilities is a benefit.

Despite some techniques have been investigated in order to estimate the measurements uncertainty (Rennie and Church, 2010; Dinehart and Burau, 2005), in this work we assume that the measured current shows a predominant velocity component that is the true velocity of the flow. The transducers are located approximately 40 centimeters below the waterline, so we have chosen an additional half-meter as blanking distance.[5] Additionally, for the purpose of gain scheduling we avoid sampling the whole column and we decided instead to set a 1-meter cell size. This means that the useful current measurements are performed in the range 90 to 190 centimeters depth. The instrument measures current velocities in each beam frame or an overall current velocity vector in its Cartesian (XYZ) frame, for each cell. The latter is then transformed to the USV BODY frame and eventually to Earth-fixed frame, as described in the Appendix.

In the following, we present two scenarios in which we have tested the gain-scheduled controller and compared that with the fixed-gains one. In the designed experiments, the USV was commanded to navigate autonomously from the fjords straight into the mouth of the river outlet (see Fig. 21). So doing, the USV would experience a negative current in its longitudinal BODY frame component ($u_c \leq 0$). Intuitively, the current would slow down the vehicle making the nominal course controller gains become ineffective. The current is measured by the ADCP and then post-processed by the onboard software, in order to extract i) its BODY frame components and ii) to compute the Earth fixed components (see Appendix), useful to provide the onshore operators with some situational awareness about the environment surrounding the USV.

[5] The blanking distance is the region immediately in front of the transducer where no measurements can be made while the transducers recover from the transmit pulse.

5.1. ADCP-based gain-scheduled steering control

In the first experiment the USV initially navigates in the surroundings of the river outlet (see Fig. 21). Fig. 22 shows the computed longitudinal current component u_c in the USV's BODY frame. It can be observed that when the USV moves away from the river mouth the perceived current is positive in the BODY frame, while it is negative when the vehicle heads towards the outlet. This confirms that the current moves outwards (North-East) as expected.

Fig. 23 shows the expected values $\hat{\gamma}$ specific to this scenario and compares them with the values (γ) computed during the sea trials. The expected values $\hat{\gamma}$ are computed by iterating through a range of ground speed (U) and heading (ψ) values chosen in a way that simulate the USV moving from North to South towards the river mouth, i.e., $U \in [0.05, 0.7]$ m/s and $\psi = \chi \in [150, 210]°$. Also, the computation of $\hat{\gamma}$ depicted in Fig. 23 assumes a sea current with constant Earth-fixed velocity $U_c = 0.5$ m/s and direction $\beta_c = 10°$, and that $\chi = \psi$ for simplicity. With the presented information it is possible to compute the NED and BODY frame velocities of the USV, its velocities relative to the water flow and hence $\hat{\gamma}$. It can be observed that γ shows values similar to the expected ones when the USV's ground speed exceeds 0.2 m/s, i.e., the points are one the surface or very close to it. When the ground speed drops some error is observed, despite the trend of the spatial distribution of γ resembles that of the expected surface (e.g., increasing γ as U decreases). The error observed at low ground speeds can be due to two main reasons: the assumptions made on the current velocity and direction, and high sensitivity to noise that affects the ground speed U and course χ measured by the onboard GNSS receiver when operating at low speeds.

Moreover, it is important to notice that the values of γ computed during the sea trials will never match exactly the surface since the current measured by the ADCP is not constant. The authors have decided to simulate γ for an average, constant current velocity $U_c = 0.5$ m/s and direction $\beta_c = 10°$ and, if one would iterate through more values of both would obtain a family of surfaces that would fit all the

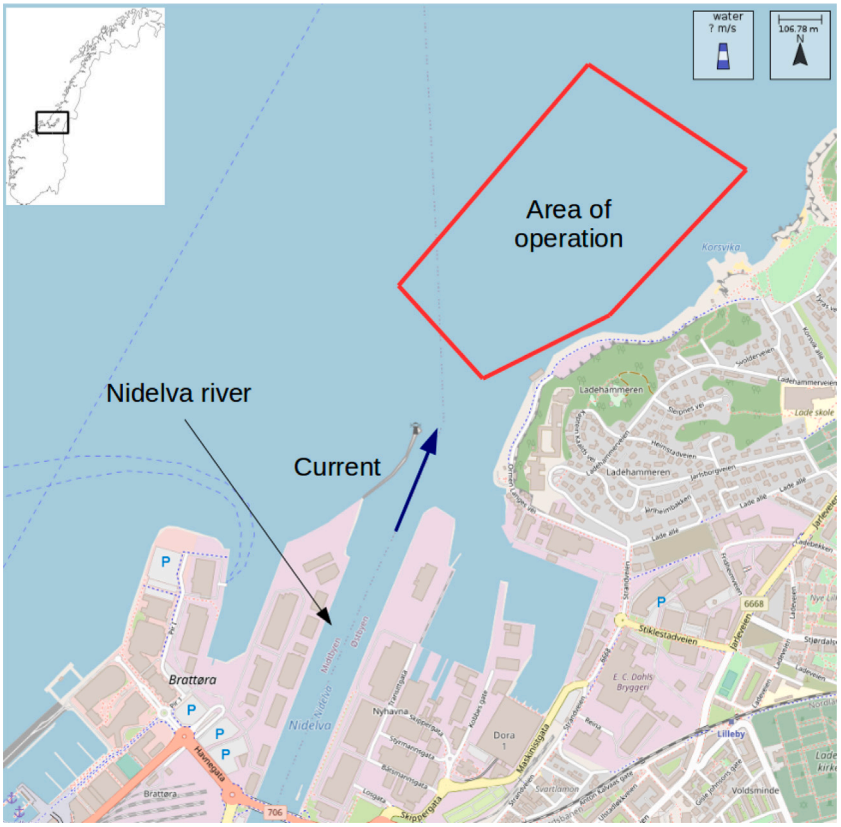

Fig. 21. USV's track in the operational area close to the mouth of the Nidelva river.

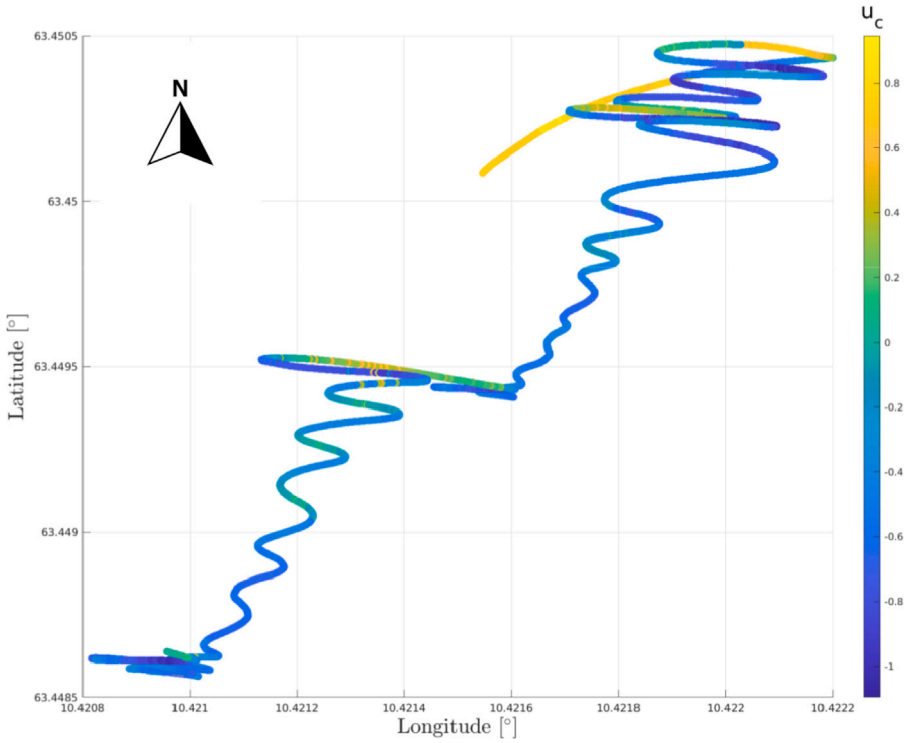

Fig. 22. USV's track while collecting current measurements at the outlet of the Nidelva river.

values computed during the sea trial. However, it is relevant to observe that the trend of γ resembles what is expected for the specific scenario.

The top graph of Fig. 24 shows the measured velocities. It can be observed that when the USV navigates with the current, then U and

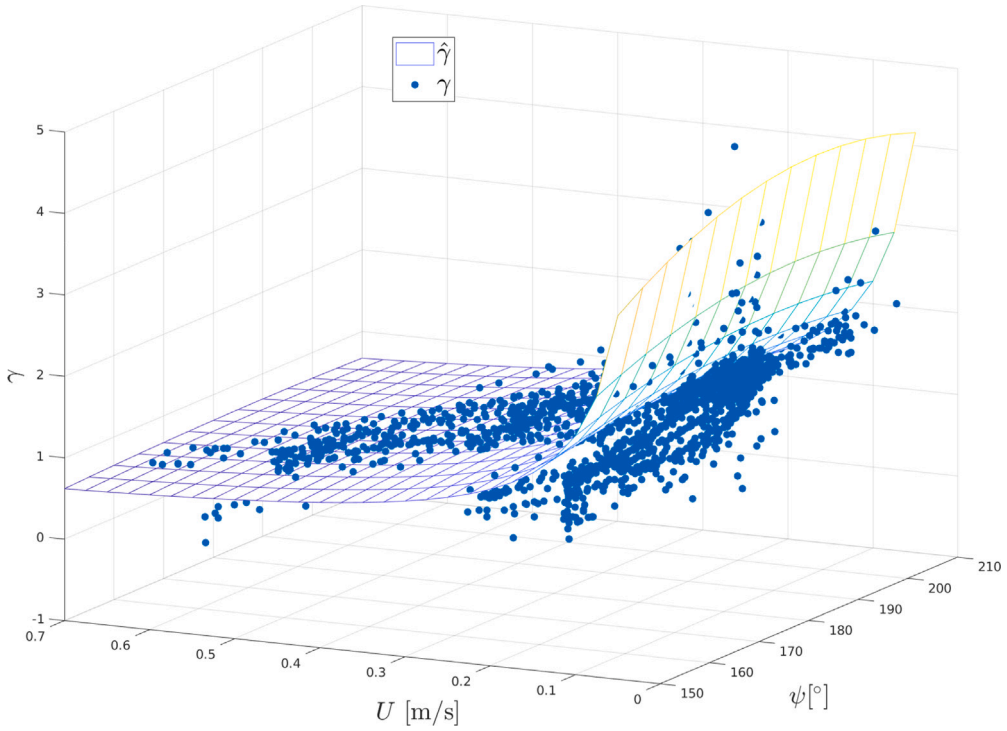

Fig. 23. Expected values $\hat{\gamma}$ and the values computed during the sea trials (γ).

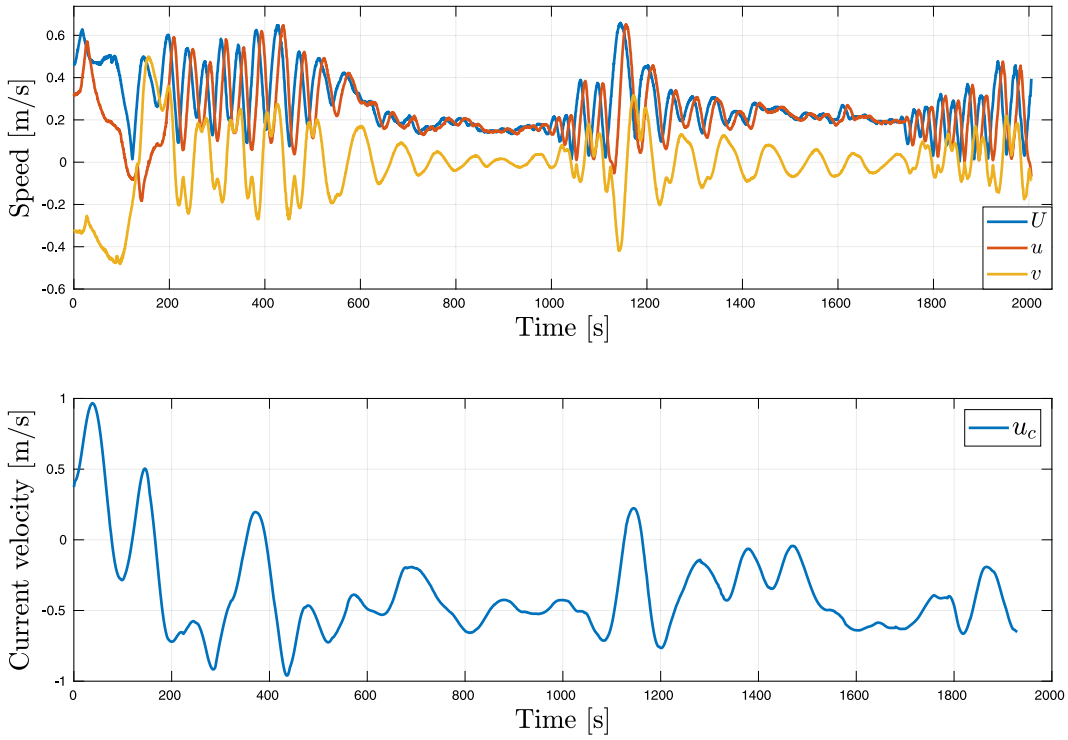

Fig. 24. Measured ground speed U and its BODY frame components u and v (top); the longitudinal current component u_c in BODY frame (bottom).

u are similar and positive. A negative lateral speed v is observed and it is due to the vehicle's heading relative to the current which is hitting its starboard side. When the USV turns around and heads towards the Nidelva outlet the longitudinal current component in the BODY frame (u_c) becomes negative and the vehicle's speed drops and oscillations are observed. This is where the nominal gains $K_p^n = 1.25$ and $K_i^n = 0.02$ become ineffective and the controller commands large rudder oscillations. The bottom graph of Fig. 24 shows the value of u_c computed based on measurements during the experiment.

Fig. 25 compares the measured course angle (χ) with the desired one (χ_d). It can be observed that large course oscillations are usually connected to large rudder angles (bottom). The red dashed lines indicate when the controller replaces the nominal gains with the scheduled ones. The reduction of the rudder efforts is clear when the scheduled

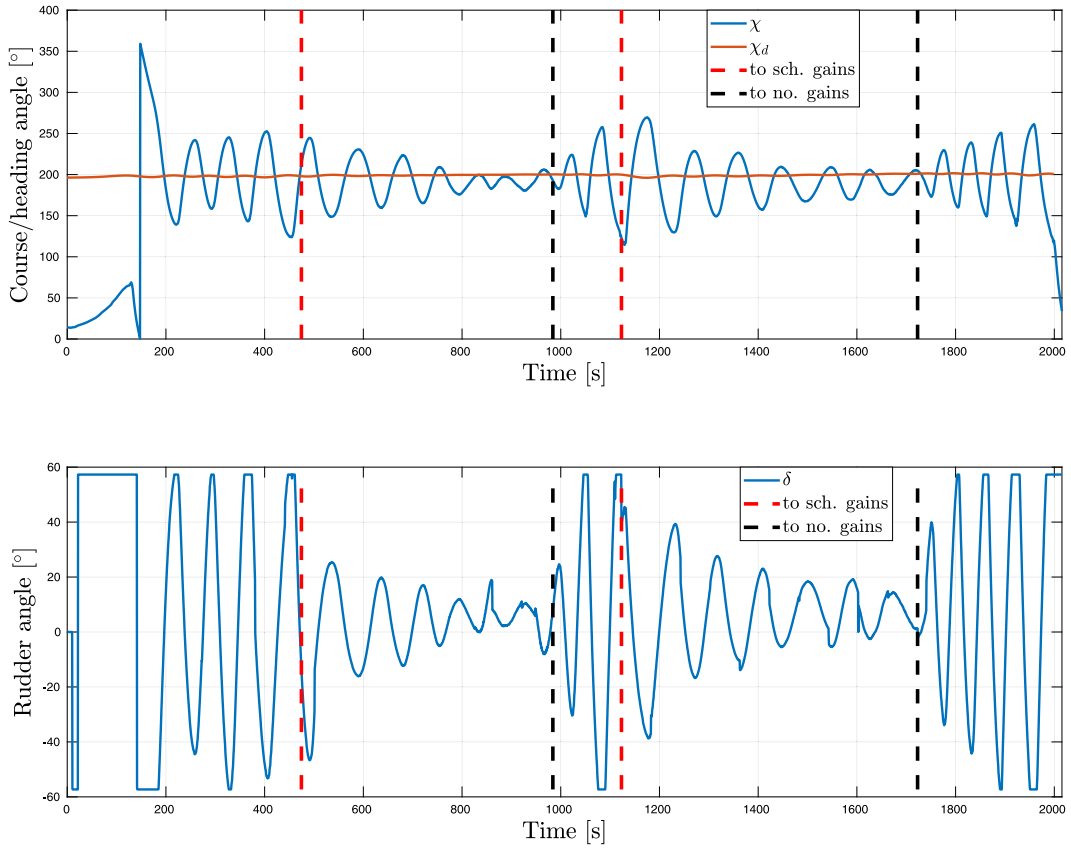

Fig. 25. Measured (χ) and desired (χ_d) course over ground (top); the computed rudder angle (δ) (bottom). Dashed lines indicate switching to gain-scheduled (red) and nominal (black) course controller. (For interpretation of the references to color in this figure legend, the reader is referred to the web version of this article.)

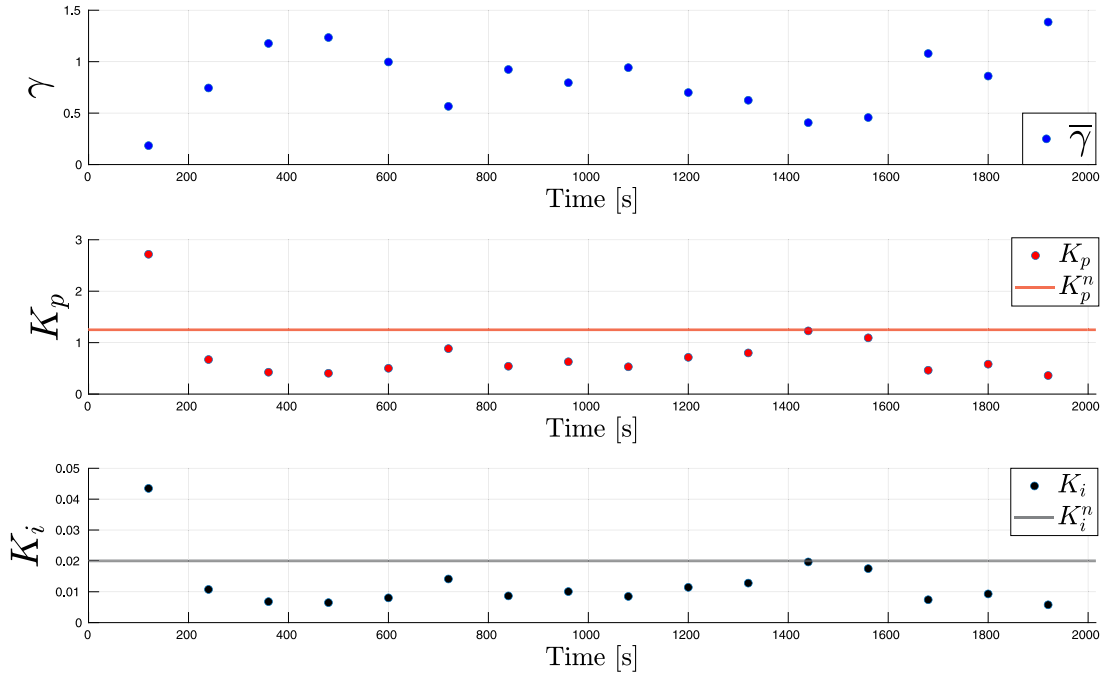

Fig. 26. Average $\bar{\gamma}$ (top); the nominal (K_p^n) and scheduled (K_p) proportional gain (middle); the nominal (K_i^n) and scheduled (K_i) integral gain (bottom).

gains are applied at time $t = 474$ s and $t = 1123$ s. As the rudder angle is reduced, an attenuation of the amplitude of course oscillations can be observed. Fig. 25 clearly indicates that the nominal gains that have been employed extensively for controlling the USV in a number of missions (Dallolio et al., 2022) involve large rudder oscillations when a sea current is experienced in the same order of magnitude of the vehicle's speed. The gain scheduling approach based on ADCP data is capable of reducing the rudder effort and produce a more efficient

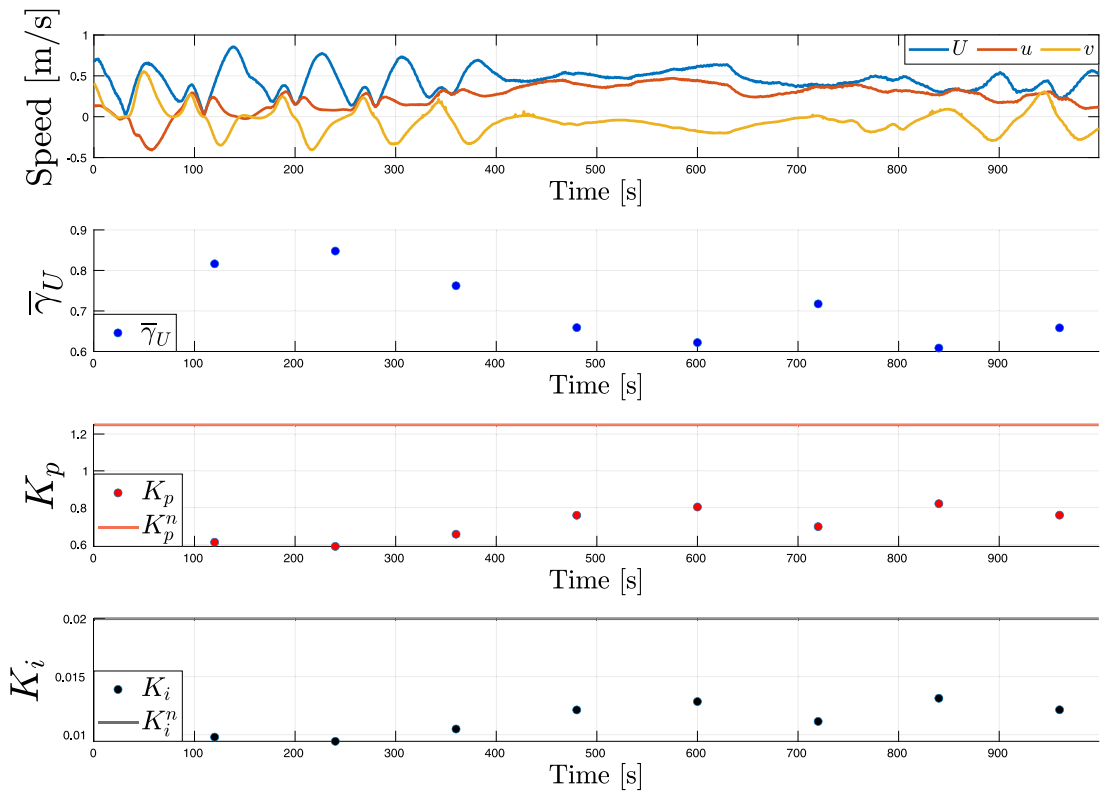

Fig. 27. Measured ground speed U and its BODY frame components u and v (top), the average $\overline{\gamma}_U$ (middle); the nominal (K_p^n) and scheduled (K_p) proportional gain (middle); the nominal (K_i^n) and scheduled (K_i) integral gain (bottom).

navigation in the desired direction. The effects of gain scheduling of the rudder control signal can also be appreciated in the measured USV's pattern. The top graph of Fig. 24 shows that when the gains are scheduled, the longitudinal speed (u) and the ground (U) speeds converge to the same values meaning no crab angle, while the lateral vehicle speed oscillates and eventually settles around 0 m/s. When the nominal gains are employed, however, larger course oscillations imply higher variation in the lateral speed as well.Fig. 26 shows the gains computed based on γ, as indicated in Eq. (9). Periodically (every 2 min), an average $\overline{\gamma}$ is computed and used to update the scheduled gains. A new computation of the gains does not indicate when the controller actually uses them: the choice of switching to nominal or scheduled gains (see Fig. 25) is left to the operators for this initial experiment.

5.2. SOG-based gain-scheduled steering control

In this section we evaluate the performances of the gain scheduling approach when the knowledge of the sea current is not available. This implies that the computation of the scheduling variable (renamed γ_U) is based only on the USV ground velocity, see Eq. (10). The test area is the same as in the previous experiment. Again, the objective of the experiment is to quantify the benefits of gain-scheduled steering control when the USV's ground speed drops.

The top graph of Fig. 27 depicts the measured ground speed (U) and the BODY frame longitudinal (u) and lateral (v) velocities. Right below, it shows the periodical average ($\overline{\gamma}_U$) used to compute the scheduled gains. It can be observed that there are relatively large U oscillations measured until time $t = 400$ s and from time $t = 800$ s to the end of the mission. It can be noticed that such oscillations are partially followed by oscillations of u and v. Fig. 27 also shows the proportional and integral gains that are computed using $\overline{\gamma}_U$.
Fig. 28 compares the measured (χ) and desired (χ_d) course angles. Large course oscillations are caused by large rudder angles (bottom). The red dashed lines indicate when the controller replaces the nominal gains with the scheduled ones. The reduction of the rudder efforts is evident when the scheduled gains are applied at time $t = 400$ s. As the rudder angle is reduced, an attenuation of the amplitude of course oscillations can be observed. Not only the course over ground stabilizes, but also the speed over ground does (see Fig. 27), increasing the navigation performance of the vehicle in the intended direction. The gains applied at time $t = 400$ s are $K_p = 0.55$ and $K_i = 0.008$. When the gain scheduling controller is deactivated and the nominal gains are restored at time $t = 800$ s, large rudder oscillations are commanded and the course-keeping performances deteriorate.

6. Conclusions

In this article the authors have presented the gain-scheduled steering system of a wave-propelled USV, taking into account the effects of ocean currents that may lead to very low speed relative to ground and to water.
A three-state quasi-linear model gives insight into the changes in steering dynamics as a function of changing environmental conditions, which is exploited in the control design to handle singular situations that occur when the USV's speed relative to the current approaches zero. Classical control design principles are applied based on a frequency analysis of the proposed model. The same analysis confirms that robust linear course control can be further investigated and achieved by implementing a gain-scheduled course-keeping autopilot.

The presented gain scheduling approach is first studied theoretically using the pole placement technique, which supports the previous frequency analysis of the model and highlights the benefits of relaxing the controller gains. The analysis shows that the variable γ can be used to schedule the autopilot gains both when the sea current measurement is available and when it is not.

The proposed control system is initially studied with simulations, which reveal the benefits of scheduling the controller gains when the

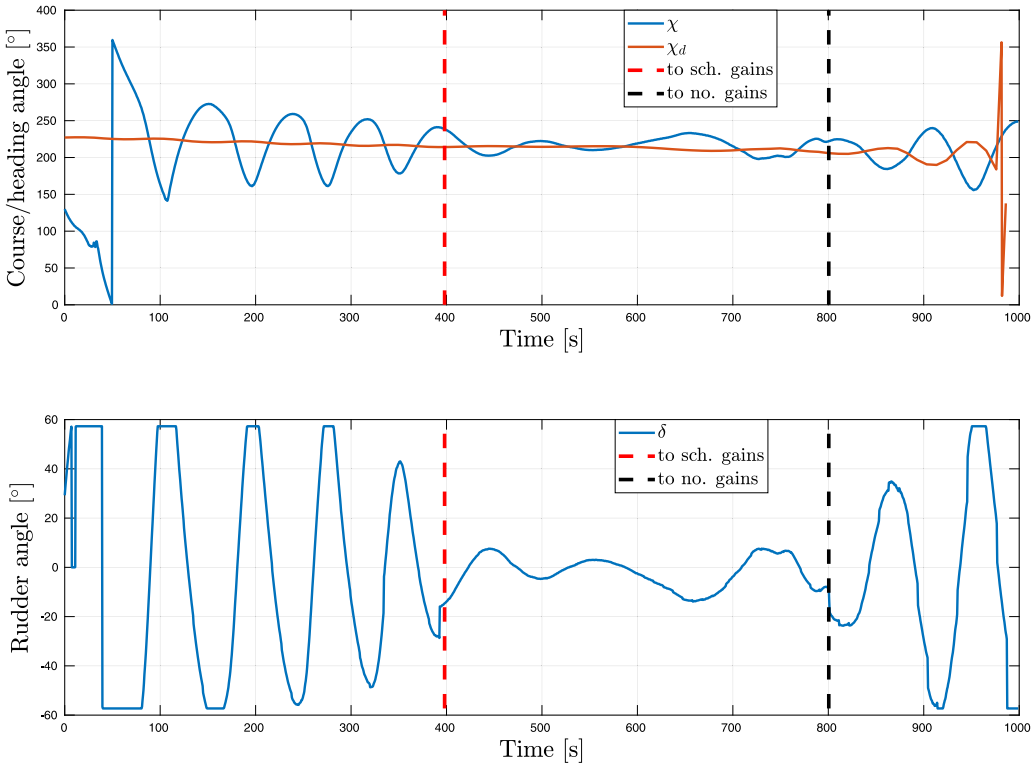

Fig. 28. Measured (χ) and desired (χ_d) course over ground (top); the computed rudder angle (δ) (bottom). Dashed lines indicate switching to gain-scheduled (red) and nominal (black) course controller. (For interpretation of the references to color in this figure legend, the reader is referred to the web version of this article.)

ocean currents appears in the same order of magnitude of the vehicle's speed.

The authors have addressed the challenges and limitations related to the ADCP instrument, before experimental results are presented based on sea trials performed in the Trondheim Fjord (Central Norway). Experimental results demonstrate that the proposed gain scheduling approach enables a more efficient navigation of the vehicle, reducing the rudder efforts and the course oscillations. Furthermore, speed oscillations are suppressed and the average velocity of the USV increases when the scheduled gains are applied. This is observed both when the ocean current measurement is available and when it is not, proving the validity of both approaches.

The authors are currently dealing with the challenge of estimating the ground speed of the USV. The benefits of a speed prediction algorithm would be observed at different levels, from course control to collision avoidance and anti-grounding. In particular, a speed prediction system could improve the gain-scheduled course control presented in this article. However, predicting the speed of a wave-propelled USV is a challenging task because of the effects that waves, winds and currents have on the vehicle.

CRediT authorship contribution statement

Alberto Dallolio: Conceptualization, Methodology, Software, Validation, Data curation, Visualization, Writing – original draft. **Henning Øveraas:** Conceptualization, Methodology, Software, Validation, Data curation, Visualization. **Tor Arne Johansen:** Conceptualization, Methodology, Validation, Supervision, Project administration, Funding acquisition.

Declaration of competing interest

The authors declare that they have no known competing financial interests or personal relationships that could have appeared to influence the work reported in this paper.

Acknowledgments

This work was supported by the Research Council of Norway (RCN) through the MASSIVE project, grant number 270959, and AMOS grant number 223254 to NTNU.

Appendix. Sea current transformations

A.1. ADCP measurements transformation

Fig. 29 shows the ADCP operating principles. The current is initially computed in the beam frame (V_n^{BEAM}). Knowing the orientation of the beams, the ADCP computes internally the Cartesian components associated to its frame. We note that, since the USV is not stationary, the measured current is not the earth-fixed stream velocity but instead the relative velocity between the USV and the flow ($U_r = \sqrt{u_r^2 + v_r^2}$). The longitudinal and lateral (u_r and v_r respectively) components of the relative speed can be used to compute the flow velocity components $u_c = u - u_r$ and $v_c = v - v_r$.

For purposes related to oceanography and marine biology, it is often useful to know the Earth-fixed direction and velocity of the planar (XY) current. These can be computed, knowing the North-East-Down (NED) components of the current, as $[N_c, E_c]^T = R[u, v]^T$, where R is the 2D rotation matrix from BODY to NED frame:

$$R = \begin{pmatrix} \cos\psi\cos\theta & \cos\psi\sin\theta\sin\phi - \sin\psi\cos\phi \\ \sin\psi\cos\theta & \cos\psi\cos\phi + \sin\psi\sin\theta\sin\phi \end{pmatrix}, \tag{11}$$

where ψ, θ and ϕ are the heading, pitch and roll angles respectively. The Earth-fixed current direction and velocity can then be computed as $\beta_c = \arctan(E_c/N_c)$ and $U_c = \sqrt{N_c^2 + E_c^2}$ respectively.

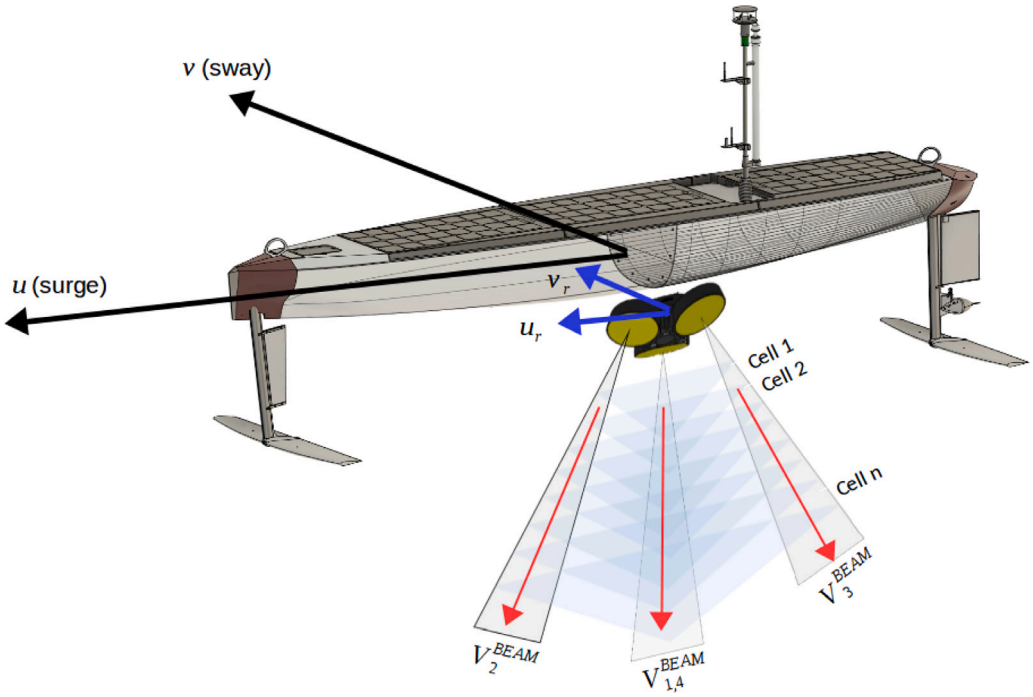

Fig. 29. ADCP sampling principle.

A.2. Sea current from Earth-fixed to BODY frame

We assume the sea current velocity in the Earth-fixed frame is denoted by U_c, while β_c is its direction relative to North. The North-East-Down (NED) components of the current are obtained as

$$N_c = U_c \cos \beta_c \tag{12}$$

$$E_c = U_c \sin \beta_c. \tag{13}$$

The current longitudinal and lateral components in the USV's BODY frame are then obtained as

$$\begin{pmatrix} u_c \\ v_c \end{pmatrix} = \begin{pmatrix} \cos\psi & -\sin\psi \\ \sin\psi & \cos\psi \end{pmatrix} \begin{pmatrix} N_c \\ E_c \end{pmatrix}. \tag{14}$$

References

Apkarian, P., Gahinet, P., 1995. A convex characterization of gain-scheduled h/sub/spl infin//controllers. IEEE Trans. Automat. Control 40, 853–864.

Camus, L., Pedersen, G., Falk-Petersen, S., Dunlop, K., Daase, M., Basedow, S.L., Bandara, K., Tverberg, V., Pederick, J., Peddie, D., Langeland, T., Cook, J., Kristiansen, T., Tjøstheim, S., Graves, I., Fietzek, P., Sperrevik, A., Christensen, K.H., Sørensen, K., Ghaffari, P., Gramvik, G., Hayes, D., Tassara, L., Aniceto, S., Aune, M., Dahle, S., 2019. Autonomous surface and underwater vehicles reveal new discoveries in the arctic ocean. In: OCEANS 2019 - Marseille. pp. 1–8.

Costa, M.J., et al., 2018. Field report: Exploring fronts with multiple robots. In: IEEE AUV. Porto.

Dallolio, A., Agdal, B., Zolich, A., Alfredsen, J.A., Johansen, T.A., 2019. Long-endurance green energy autonomous surface vehicle control architecture. In: OCEANS 2019, Seattle, Washington.

Dallolio, A., Alfredsen, J.A., Fossen, T.I., Johansen, T.A., 2021. Experimental validation of a nonlinear wave encounter frequency estimator onboard a wave-propelled USv. IFAC-PapersOnLine 54 (16), 188–194. http://dx.doi.org/10.1016/j.ifacol.2021.10.092, 13th IFAC Conference on Control Applications in Marine Systems, Robotics, and Vehicles CAMS 2021 URL https://www.sciencedirect.com/science/article/pii/S2405896321014944.

Dallolio, A., Øveraas, H., A. Alfredsen, J., I. Fossen, T., A. Johansen, T., 2022. Design and validation of a course control system for a wave-propelled unmanned surface vehicle. Field Robotics Volume 2, 748–773. http://dx.doi.org/10.55417/fr.2022025.

Dinehart, R.L., Burau, J.R., 2005. Averaged indicators of secondary flow in repeated acoustic Doppler current profiler crossings of bends. Water Resour. Res. 41, 09405.

Ferreira, A.S., Costa, M., Py, F., Pinto, J., Silva, M.A., Nimmo-Smith, A., Johansen, T.A., de Sousa, J.a.B., Rajan, K., 2018. Advancing multi-vehicle deployments in oceanographic field experiments. Auton. Robots http://dx.doi.org/10.1007/s10514-018-9810-x.

Fossen, T., 2021. Handbook of Marine Craft Hydrodynamics and Motion Control, 2nd ed. Wiley.

Glenn, S., Kohut, J., McDonnell, J., Seidel, D., Aragon, D., Haskins, T., Handel, E., Haldeman, C., Heifetz, I., Kerfoot, J., Lemus, E., Lictenwalder, S., Ojanen, L., Roarty, H., Students, A.C., Jones, C., Webb, D., Schofield, O., 2011. The trans-atlantic slocum glider expeditions: A catalyst for undergraduate participation in ocean science and technology. Mar. Technol. Soc. 45, 75–90.

Hine, R., Willcox, S., Hine, G., Richardson, T., 2009. The wave glider: A wave-powered autonomous marine vehicle. In: OCEANS 2009. pp. 1–6. http://dx.doi.org/10.23919/OCEANS.2009.5422129.

Johnston, P., Poole, M., 2017. Marine surveillance capabilities of the AutoNaut wave-propelled unmanned surface vessel (USv). In: OCEANS 2017 - Aberdeen. pp. 1–46. http://dx.doi.org/10.1109/OCEANSE.2017.8084782.

Khalil, H.K., 2002. Nonlinear Systems; 3rd Ed.. Prentice-Hall, Upper Saddle River, NJ.

Kim, D., Yu, K., 2010. Uncertainty estimation of the ADCP velocity measurements from the moving vessel method, (I) development of the framework. KSCE J. Civ. Eng. 14, 797–801. http://dx.doi.org/10.1007/s12205-010-0950-6.

Kragelund, S., Dobrokhodov, V., Monarrez, A., Hurban, M., Khol, C., 2013. Adaptive speed control for autonomous surface vessels. In: OCEANS 2013 MTS/IEEE - San Diego: An Ocean in Common.

Leith, D., Leithead, W., 2000. Survey of gain-scheduling analysis and design. Internat. J. Control 73, 1001–1025. http://dx.doi.org/10.1080/002071700411304.

McGillivary, P., Borges de Sousa, J., Martins, R., Rajan, K., Leroy, F., 2012. Integrating autonomous underwater vessels, surface vessels and aircraft as persistent surveillance components of ocean observing studies. In: 2012 IEEE/OES Autonomous Underwater Vehicles (AUV). pp. 1–5. http://dx.doi.org/10.1109/AUV.2012.6380734.

Peimin, Z., Huajun, Z., Xinchi, T., 2018. The design of gain scheduling PID controller of the USv course control system. In: 2018 Chinese Automation Congress. CAC, pp. 1408–1413. http://dx.doi.org/10.1109/CAC.2018.8623062.

Rennie, C., Church, M., 2010. Mapping spatial distributions of uncertainty of water and sediment flux in large gravel-bed river reach using an aDcp. J. Geophys. Res. 115, http://dx.doi.org/10.1029/2009JF001556.

Rugh, W.J., Shamma, J.S., 2000. Research on gain scheduling. Automatica 36 (10), 1401–1425.

dos Santos, D.H., Goncalves, L.M.G., 2019. A gain-scheduling control strategy and short-term path optimization with genetic algorithm for autonomous navigation of a sailboat robot. Int. J. Adv. Robot. Syst. 16 (1), 1729881418821830. http://dx.doi.org/10.1177/1729881418821830, arXiv:10.1177/1729881418821830.

Santos, D., Negreiros, A., Jacobo, J., Goncalves, L., Silva Junior, A., Silva, J.M., 2018. Gain-scheduling PID low-level control for robotic sailboats. In: 2018 Latin American Robotic Symposium, 2018 Brazilian Symposium on Robotics (SBR) and

2018 Workshop on Robotics in Education. WRE, pp. 147–152. http://dx.doi.org/10.1109/LARS/SBR/WRE.2018.00035.

Shamma, J., Athans, M., 1990. Analysis of gain scheduled control for nonlinear plants. IEEE Trans. Automat. Control 35 (8), 898–907.

Shamma, J.S., Athans, M., 1991. Guaranteed properties of gain scheduled control for linear parameter-varying plants. Automatica 27 (3), 559–564.

Shamma, J.S., Athans, M., 1992. Gain scheduling: Potential hazards and possible remedies. IEEE Control Syst. Mag. 12 (3), 101–107.

Smith, R.N., Schwager, M., Smith, S.L., Jones, B.H., Rus, D., Sukhatme, G.S., 2011. Persistent ocean monitoring with underwater gliders: Adapting sampling resolution. J. Field Robotics 28 (5), 714–741, URL http://cres.usc.edu/cgi-bin/print_pub_details.pl?pubid=710.